



## Structure, mechanical and tribological properties, and oxidation resistance of TaC/a-C:H films deposited by high power impulse magnetron sputtering

Huan Luo, Mohammad Arab Pour Yazdi, Sheng-Chi Chen, Hui Sun, Fei Gao, Olivier Heintz, Alexis de Monteynard, Frédéric Sanchette, Alain Billard

### ► To cite this version:

Huan Luo, Mohammad Arab Pour Yazdi, Sheng-Chi Chen, Hui Sun, Fei Gao, et al.. Structure, mechanical and tribological properties, and oxidation resistance of TaC/a-C:H films deposited by high power impulse magnetron sputtering. *Ceramics International*, 2020, 46, pp.24986 - 25000. 10.1016/j.ceramint.2020.06.284 . hal-03491969

**HAL Id: hal-03491969**

**<https://hal.science/hal-03491969>**

Submitted on 26 Sep 2022

**HAL** is a multi-disciplinary open access archive for the deposit and dissemination of scientific research documents, whether they are published or not. The documents may come from teaching and research institutions in France or abroad, or from public or private research centers.

L'archive ouverte pluridisciplinaire **HAL**, est destinée au dépôt et à la diffusion de documents scientifiques de niveau recherche, publiés ou non, émanant des établissements d'enseignement et de recherche français ou étrangers, des laboratoires publics ou privés.



Distributed under a Creative Commons Attribution - NonCommercial 4.0 International License

## **Structure, mechanical and tribological properties, and oxidation resistance of TaC/a-C:H films deposited by high power impulse magnetron sputtering**

Huan Luo<sup>1,\*</sup>, Mohammad Arab Pour Yazdi<sup>1</sup>, Sheng-Chi Chen<sup>2,3</sup>, Hui Sun<sup>4,\*</sup>, Fei Gao<sup>5</sup>, Olivier Heintz<sup>6</sup>, Alexis de Monteynard<sup>7</sup>, Frédéric Sanchette<sup>7</sup>, Alain Billard<sup>1</sup>

<sup>1</sup> FEMTO-ST, UMR 6174 CNRS, MN2S, Univ. Bourgogne Franche-Comté, UTBM, Site de Montbéliard, 90000 Belfort Cedex, France

<sup>2</sup> Department of Materials Engineering and Center for Plasma and Thin Film Technologies, Ming Chi University of Technology, Taipei 243, Taiwan

<sup>3</sup> College of Engineering, Chang Gung University, Taoyuan 333, Taiwan

<sup>4</sup> Shandong Key Laboratory of Optical Astronomy and Solar-Terrestrial Environment, School of Space Science and Physics, Shandong University, Weihai, Shandong, 264209, China

<sup>5</sup> FEMTO-ST, UMR 6174 CNRS, Energy Department, Univ. Bourgogne Franche-Comté, UTBM, Rue Thierry Mieg, 90000 Belfort Cedex, France

<sup>6</sup> ICB, UMR 6303 CNRS, Université Bourgogne Franche-Comté, BP 47870, 21078 Dijon Cedex, France

<sup>7</sup> Nogent International Center for CVD Innovation, LRC CEA-ICD LASMIS, UTT, Antenne de Nogent-52, Pôle Technologique de Haute-Champagne, 52800 Nogent, France

\*Corresponding authors: huan.luo@utbm.fr (Huan Luo); huisun@sdu.edu.cn (Hui Sun)

### **Abstract:**

TaC/a-C:H films with varying carbon content within a narrow window were deposited employing HiPIMS in the Ar/C<sub>2</sub>H<sub>2</sub> atmosphere. The DC deposited TaC/a-C:H reference films were prepared under the same deposition parameters for comparison. Analysis and comparison of the chemical bonding state, structure, mechanical and tribological properties, and oxidation resistance of the films were conducted, with the aim of emphasizing the differences in the nanocomposite structure and properties of the films correlated to deposition conditions. It reveals that the HiPIMS deposited TaC/a-C:H films outperform the DC deposited

ones, exhibiting higher hardness and toughness, lower friction coefficient and wear rate, and stronger oxidation resistance. The improved performances in HiPIMS are attributed to HiPIMS plasma, which enables (i) the volume fraction of crystalline TaC phase and amorphous carbon phase, (ii) the stoichiometric ratio and grain size of the crystalline phase, (iii) the  $sp^2/sp^3$  -C ratio, and (iv) the residual stress to develop in the manner that is conducive to film properties. It is demonstrated that HiPIMS plasma can be used as an effective means to modulate the chemical bonding state and nanocomposite structure of TaC/a-C:H film for achieving higher performance in terms of hard yet tough, wear and oxidation resistance.

**Keywords:** TaC/a-C:H film; Mechanical properties; Tribological performance; Oxidation resistance.

## 1. Introduction

Transition metal carbide films have been a hot topic for industrial applications and academic research for decades due to their high hardness [1][2][3], high melting point and excellent chemical stability [4][5][6][7]. Unlike the nitride system, the carbon-based film of transition metal is characterized by the nanocomposite structure consisting of two separate phases, nanocrystalline grain of carbide and amorphous carbon. Since this nanocomposite structure has a significant potential to improve the mechanical properties and wear resistance [8], the metal carbide/amorphous carbon nanocomposites are widely used as protective coatings on surfaces of precision steel components, cutting tools and machinery components [9]. Also a variety of transition metal carbide films have been extensively studied, such as WC/a-C:H [10][11], TiC/a-C:H [8][12][13], NbC/a-C:H [14][15], ZrC/a-C:H [16].

Among transition metal carbides, tantalum carbide (TaC) has attracted considerable attention since it has high hardness, good thermal stability, high melting temperature (3880 °C), low contact resistance, and excellent tribological performance. Based on its superior performance and promising applications in industry, nanocomposite TaC coatings have been prepared and studied by a variety of modern surface modification technologies, such as hot pressing [17], magnetron sputtering [1][18][19][20][21][22][23], in situ reaction (ISR) technique [24][25], carburization [26][27], pulsed laser ablation deposition [28][29][30], chemical vapor deposition [31][32], electrodeposition [33] and so on. Among them, one of the most widely used techniques to grow TaC films is direct current (DC) magnetron sputtering. Du, S. and Zhang, K. et al. [19]

studied the mechanical properties and tribological behavior of the TaC coatings prepared by reactive DC magnetron sputtering, and reached a maximum hardness of 36.3 GPa and the lowest wear rate of  $1.44 \times 10^{-6} \text{ mm}^3/\text{Nm}$ . Evans, R. D. *et al.* [20][21] investigated the influence of deposition parameters on the composition and structure of TaC/a-C:H films in the reactive direct current magnetron sputtering, including acetylene flow rate, applied bias voltage, and substrate rotation rate. Poladi, A. *et al.* [23] studied the effect of C content on the structural, mechanical, wear and corrosion properties of TaC films via DC magnetron sputtering. They showed that ceramic TaC films (20 at.% of C content) exhibit optimal mechanical properties and wear resistance, and metallic Ta(C) films (lower 10 at.% C content) exhibit the best corrosion resistance. Moreover, Cai, X., Xu, Y. *et al.* [24] fabricated a gradient nanostructured TaC layer by in situ reaction. The hardness of 28.1 GPa and the fracture toughness of  $3.9 \pm 0.2 \text{ MPa m}^{1/2}$  were obtained at the topmost surface of the TaC layer. Zhao, N. *et al.* [25] studied the TaC coating synthesized by in situ synthesis and combined casting-heat treatment, and analyzed the thermodynamics, kinetics and atomic diffusion of the coating formation. It demonstrated that the thickness of the carbide layer has a parabolic relationship with the treatment time, and the activation energy for the process was 388.68 kJ/mol. Zhao, Z. *et al.* [26] fabricated TaC coatings on tantalum by interstitial carburization and studied their mechanical properties and scratch resistance performance. The TaC coating (1900 HV) with hardness 14 times higher than that of the Ta substrate (137 HV) was successfully prepared. In addition, Hackett, K. *et al.* [17] studied the phase constitution and mechanical properties of the Ta-C system via hot-pressing mixed powders of TaC and Ta. It demonstrated that the grain size decreased with increasing carbon content, with a corresponding increase in Vickers hardness from 13.5 to 20 GPa. Teghil, R. *et al.* [28] investigated the TaC films prepared by a frequency-doubled Nd: glass laser, and proposed an ablation deposition mechanism (related to target thermal particle spraying) to explain the film features.

However, although a variety of advanced surface techniques have been applied to the preparation of tantalum carbide films as reviewed above, to the best of our knowledge, the TaC/a-C:H film prepared via HiPIMS has never been studied. HiPIMS is an advanced physical vapor deposition technology, especially for the fields of protective films and functional films, known for its high power density and high ionization rate during the discharge. Inspired by its plasma characteristics, in the present work, we attempt to employ it to

tune the (i) chemical bonding state, (ii) volume ratio of amorphous carbon matrix to crystalline phase, (iii) ratio  $sp^3/sp^2$ -C, and (iv) stoichiometric ratio  $x$  (of  $TaC_x$  grains) of the nanocomposite TaC/a-C:H films. These four points have a crucial impact on the hardness, toughness and tribological properties of the film. Especially toughness, it is lacking in transition metal carbide films. Poor toughness is detrimental when subjected to high load and/or long-term friction conditions since the possibility of fracture failure (which causes catastrophic damage to wear resistance). In addition, as is generally known, the plasma characteristics of HiPIMS can also adjust (i) the grain size and (ii) the compactness of the film morphology, [which is conducive to mechanical properties](#). Therefore, the research on the nanocomposite structure and properties of [the](#) TaC/a-C:H film deposited by HiPIMS is worth looking forward to.

Moreover, when the TaC/a-C:H film is used as the protective coating, the high-temperature environment cannot be avoided. The anti-oxidation capability of the film is thus critical as it limits the application scope, efficiency [and service life](#). However, [the investigation of the](#) oxidation resistance of TaC/a-C:H film [is](#) rarely explored. Besides, [the research on TaC/a-C:H film in the publication](#) has mainly focused on the effect of [the](#) carbon content varying over a wide range (from pure nanocrystalline TaC without amorphous carbon phase to almost pure amorphous diamond-like carbon (i.e., doped with Ta atoms)) on the properties of the film. The disadvantage is that [a large change](#) in carbon content may [obscure](#) other factors contributing to the film performance. The effect of [the carbon content varying within a narrow range](#) on the structure and properties of the TaC/a-C:H film is rarely studied.

Trying to explore the above issues, a series of TaC/a-C:H films were prepared in HiPIMS, operated at three substrate biases (floating, -50 V, and -100 V), by varying the flow rate of acetylene ( $C_2H_2$ ). For comparison, TaC/a-C:H films were also prepared in DC magnetron sputtering (without substrate bias) with the same deposition parameters. The chemical bonding state, microstructure, morphology, residual stress, mechanical properties, and tribological performance as well as oxidation resistance of all the TaC/a-C:H films were characterized. By comparing the TaC/a-C:H films deposited in different deposition conditions (DC and HiPIMS with different substrate bias modes), [the correlation](#) between [the](#) deposition conditions and [the](#) nanocomposite structure, mechanical properties, tribological behavior and oxidation resistance of TaC/a-C:H films [were](#) systematically discussed and established.

## 2. Experimental details

### 2.1. Films deposition

TaC/a-C:H films were prepared via HiPIMS (Hüttinger Elektronik Generator 4002) by sputtering a tantalum target (150 mm in diameter and 8 mm in thickness, 99.9 % purity) in the Ar and C<sub>2</sub>H<sub>2</sub> gas mixture. The cathode discharge parameters were set to: U = -600 V (during pulse time-on), I = 2.2 A (average current), t<sub>on</sub> = 45 μs, f = 500 Hz. The potential of the substrate holder was operated at three modes: floating, -50 V, -100 V bias. The reference films were deposited by DC (Pinnacle Plus, Advanced Energy) with the average current of 2.2 A, f = 50 KHz and T<sub>off</sub> = 5 μs. Except for the power supply, other deposition parameters are the same as in HiPIMS. M2 disc substrate (63 HRC, Ø=30 mm × 8 mm), stainless steel slide (40 mm×20 mm×4 mm), silicon wafer (10 mm×10 mm) and iron sheet (400 mm×4 mm×0.25 mm) were selected as the substrates for testing mechanical properties, tribological performance, morphology, chemical bonding states, and residual stress. The substrates of M2 and stainless steel were mirror polished with a diamond suspension of 1 μm of granulometry and degreased in ethanol afterward.

Prior to film deposition, the vacuum chamber was pumped down to a base pressure ~10<sup>-4</sup> Pa. The substrates were etched for ten minutes to remove adventitious contaminants attached to their surfaces. Subsequently, a tantalum interlayer of approximately 200 nm thickness was pre-deposited between the TaC/a-C:H film and the substrate to improve the film adhesion. During the deposition of all batches, the working pressure was 0.4 Pa. The distance between the substrate holder and the target D<sub>t-s</sub> was 10 cm. The flow rates of Ar and C<sub>2</sub>H<sub>2</sub> were controlled by mass flow controllers. The flow rate of Ar was maintained at 200 sccm and of C<sub>2</sub>H<sub>2</sub> was varied from 10 sccm to 18 sccm with 2 sccm step increments. To obtain homogeneous films, the rotating substrate holder was fixed at the speed of 30 revolutions per minute (r.p.m.).

### 2.2. Characterization

The film microstructure was performed by Bragg Brentano configuration X-ray diffraction (BRUKER D8), which is equipped with a Co (λ=1.78897 Å) source at a voltage of 35 kV and a current of 40 mA. Film morphologies on the top surface and brittle fracture cross-section were observed by JEOL JSM-7800F field emission gun scanning electron microscope (FEG-SEM). The chemical bonding states of TaC/a-C:H films were analyzed by X-ray photoelectron spectroscopy (XPS) in an attempt to reveal the intrinsic origin of the excellent

performance of the film. It was performed under an ultra-high vacuum ( $\sim 10^{-8}$  Pa) with an Al K $\alpha$  X-ray source ( $h\nu=1486.7$  eV). Charge calibration was performed by setting the binding energy of the C 1s photoelectron peak to 285 eV.

The nanohardness and Young's modulus of the film were measured by using the Nanoindentation Tester from CSM Instruments equipped with the Berkovich diamond indenter tip at room temperature. Final results were determined based on the Oliver&Pharr model and were the average value of 12 indentations performed for each sample. In order to avoid the influence of the substrate on the measurement results, the penetration depth of the indenter was kept <10% of the thickness of the film. The residual stress inside the films was calculated via the Stoney formula:

$$\sigma = \frac{E_s}{6(1-\nu_s)} \frac{d_s^2}{d_f R} \quad (1)$$

in which  $E_s$ ,  $d_s$ , and  $\nu_s$  represent Young's modulus, thickness, and Poisson's ratio of the substrate, respectively.  $d_f$  stands for the thickness of the film.  $R$  represents the radius of curvature, which is measured from the film as-deposited on a cantilever beam by Altysurf profilometer equipped with an optical probe.

The tribological performance of the film was carried out by a pin-on-disk Tribometer (CSM, Switzerland). All pin-on-disk measurements were done via unlubricated sliding against 6 mm WC/Co ball in ambient air at a relative humidity of about 40 %. Test parameters were set to 5 N applied normal load, 1.6 cm/s sliding speed, 3 mm contact track radius and 10000 sliding laps. After the tribological test, the cross-sectional profile of the wear track was characterized by an Altysurf profilometer equipped with an inductive probe. The normalized wear rate ( $W_r$ ) was calculated using equation  $W_r=V/(L \times S)$ , where  $V$  is the wear volume,  $L$  is the applied normal load, and  $S$  is the sliding distance. The wear track on the M2 substrate was observed by SEM. Annealing treatment was performed under air atmosphere at different temperatures (from 200 °C up to 700 °C with an incremental step of 100 °C) with a dwell time of 2 h to test the oxidation resistance of the film. The oxidation degree of the film after annealing was measured by XRD, SEM, and energy dispersive X-ray spectroscopy (EDS).

### 3. Results and discussions

#### 3.1 Chemical bonding state

Fig. 1 shows high resolution XPS spectra C 1s of TaC/a-C:H films deposited in different conditions: DC and HiPIMS (shown in (a) and (b)), as well as HiPIMS with different substrate bias (shown in (c)). The C 1s peak exhibits four main components distributed at 282.8 eV (Ta-C), 284.5 eV ( $sp^2$ -C), 285.4 eV ( $sp^3$ -C) and 286.8 eV (C-O). Table 1 lists the stoichiometric ratio  $x$  of  $TaC_x$  grains and the fractions of Ta-C,  $sp^2$ -C,  $sp^3$ -C bonds, which are determined by the relative peak areas of the fitted peaks. Note that in Table 1, the samples are named TaC10, TaC12, TaC14, TaC16, TaC18, respectively, according to the flow rate of  $C_2H_2$  used in the film formation process.

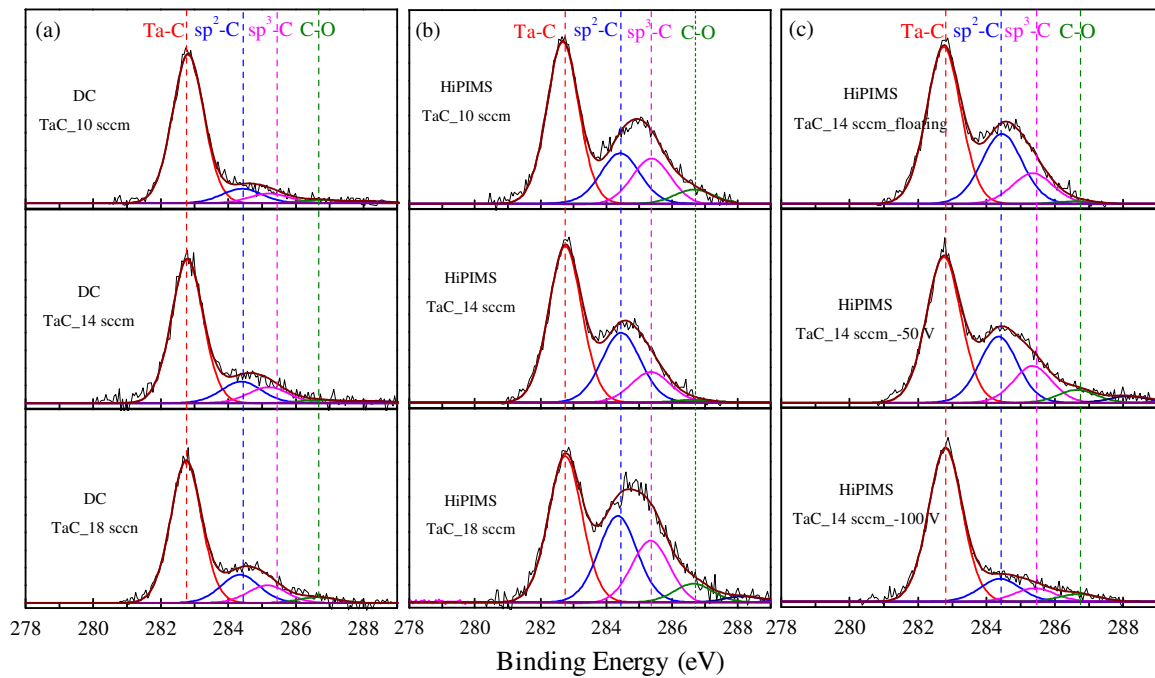


Figure 1. High resolution XPS spectra C 1s of TaC/a-C:H films deposited in different conditions: (a) DC; (b) HiPIMS with floating substrate; (c) HiPIMS with substrate bias.

From Fig. 1 and Table 1, two different evolutionary trends of carbide Ta-C and amorphous carbon can be observed. One is that as the  $C_2H_2$  flow rate grows, the content of Ta-C bond is decreased, and the amorphous carbon content ( $sp^2$ -C and  $sp^3$ -C bonds) is gradually increased in both DC and HiPIMS. Further information on the amorphous carbon phase is the continuous increase in  $sp^2$ -C bond and the random variation in  $sp^3$ -C bond with the increasing  $C_2H_2$ . For DC deposited films, as the  $C_2H_2$  flow rate increases, the content of Ta-C bond

decreases from 77.4 to 69.3 at.%, and the  $sp^2$ -C bond rises from 16.2 to 20.6 at.%. For HiPIMS deposited films, the Ta-C bond decreases from 55.3 to 44.4 at.%, while the  $sp^2$ -C bond rises from 21.2 to 30.6 at.%. There is no regular change in the content of  $sp^3$ -C bond as the  $C_2H_2$  flow rate increases in DC and HiPIMS. It fluctuates randomly within a small range and remains stable at 9.1 at.% and 22.4 at.% for DC films and HiPIMS films, respectively. The stoichiometric ratio of TaC/a-C:H film ( $x$  in  $TaC_x$ ) increases with the  $C_2H_2$  flow rate in both DC and HiPIMS. From 10 to 18 sccm,  $x$  increases from 0.45 to 0.69 for DC films and from 0.65 to 0.78 for HiPIMS film.

Comparing the C 1s peaks of DC and HiPIMS deposited films, the C incorporation in HiPIMS deposited films is higher, characterized by the higher stoichiometric ratio and the higher amorphous carbon content. Since HiPIMS plasma has higher energy density and higher ionization rate, which enhances the reactivity between Ta and C not only in the discharge process, but also on the growth interface of the film, a higher content of C is incorporated into the film [35]. Similar results have also been observed by Souček, P. *et al.* [36], which showed that approximately 2-3 times higher acetylene flow is required to deposit TiC/a-C:H films with the same composition in DCMS as in HiPIMS.

The other is that as the substrate bias increases in HiPIMS, the content of Ta-C bond increases, while the contents of  $sp^2$ -C and  $sp^3$ -C bonds decrease. It is consistent with the result in [21]. The increased Ta-C bond is due to the fact that Ta ions can obtain more kinetic energy from the acceleration of the biased substrate (due to their mass advantages) when they eject from the target and bombard the substrate. The higher kinetic energy results in Ta and C to react as completely as possible at the growing interface of the film, thereby increasing the Ta-C bond. As another result of higher bombardment energy, the stoichiometric ratio of TaC grains increases with the substrate bias.

Table 1. The relative amount of chemical bonds of Ta-C,  $sp^2$ -C and  $sp^3$ -C, stoichiometric ratio  $x$  of TaC grains, and amorphous carbon content of the TaC/a-C:H films with different  $C_2H_2$  flow rates.

Batch no.	Composition		Types of bonding for C 1s XPS			a-C:H [at.%]	Stoichiometric ratio $x$ (TaC $_x$ )
	[at.%]		[at.%]				
	Ta	C	C-Ta	sp <sup>2</sup> -C	sp <sup>3</sup> -C		
DC							

TaC10	63.5	36.5	77.4	16.2	6.4	8.3	0.45
TaC12	59.9	40.1	75.1	14.3	10.6	10.0	0.50
TaC14	55.3	44.7	71.3	17.7	11.0	12.8	0.58
TaC16	52.6	47.4	72.8	20.0	7.2	13.0	0.66
TaC18	50.2	49.8	69.3	20.6	10.1	15.3	0.69
HiPIMS_floating substrate							
TaC10	46.2	53.8	55.3	21.2	23.5	24.0	0.65
TaC12	44.0	56.0	55.2	24.1	20.7	25.1	0.70
TaC14	41.6	58.4	53.0	24.7	22.3	27.4	0.74
TaC16	39.7	60.3	50.4	29.0	20.6	29.9	0.77
TaC18	36.3	63.7	44.4	30.6	25.0	35.4	0.78
HiPIMS_substrate bias							
TaC12-50V	48.7	51.3	67.4	15.2	17.4	16.7	0.71
TaC12-100V	52.9	47.1	82.0	12.1	5.9	8.5	0.73
TaC14-50V	44.3	55.7	55.1	25.7	19.2	25.0	0.69
TaC14-100V	48.7	51.3	73.6	13.9	12.5	13.5	0.77
TaC16-50V	42.6	57.4	58.5	21.9	19.6	23.8	0.79
TaC16-100V	49.0	51.0	78.0	13.8	8.2	11.2	0.81

Typically, the enhanced bombardment energy of film-forming plasma leads to higher crystallinity, larger grain size and higher  $sp^3$ -C content in the amorphous carbon matrix. However, the content of  $sp^3$ -C is lowered in our case. It is because the greatly increased Ta-C bond occupies too much C source. Under this condition, although the enhanced bombardment energy provided by substrate bias induces the subsurface penetration and compressive stress as well (which facilitates the formation of  $sp^3$ -C), the remaining carbon may not be sufficient to support the increase of  $sp^3$ -C content. Based on the above analysis, it can be concluded that the evolution of the chemical bonding state is not only related to the composition of the plasma which has been reported several times in the literature [34][37], but also strongly depends on the ionization rate and bombardment energy of the plasma. This indicates that HiPIMS can provide a more flexible modulation in terms of the chemical bonding state of the TaC/a-C:H film through two auxiliary means of plasma energy and ionization rate. Moreover, it is expected that the HiPIMS-modulated chemical bonding state allows TaC/a-C:H film to achieve superior performance that is often unachievable in the other PVD approaches.

### 3.2 Morphology and Microstructure

Fig. 2 exhibits the SEM micrographs of fracture cross-sections and top surfaces (inserted in the upper right corner) of the TaC/a-C:H films deposited with different  $C_2H_2$  flow rates. The upper and lower rows represent

the results of the films deposited in DC and HiPIMS (floating), respectively. As the  $C_2H_2$  flow rate increases, all DC deposited films exhibit glassy morphology, while all HiPIMS deposited films display columnar structure characteristics. The columns of HiPIMS deposited films do not change with the  $C_2H_2$  flow rate, exhibiting a very similar density. The difference in cross-sectional morphologies between DC and HiPIMS deposited films is contrary to what is commonly reported in the literature [38][39]. We notice that in HiPIMS deposition condition, the ionization rate of film-forming plasma is higher. The motion path of ions is thus highly oriented and almost perpendicular to the substrate surface due to the attraction of the floating potential of the substrate. Under this plasma characteristic, the film is grown by the rapid, continuous and normally incident species, thereby forming a compact columnar structure perpendicular to the substrate [40].

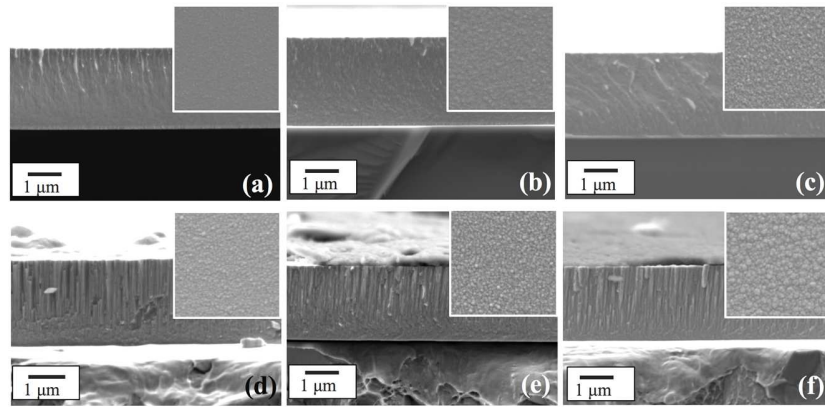


Figure 2. SEM micrographs of cross-sections and top surfaces (upper right corner) of TaC/a-C:H films deposited in DC (upper row, a-c) and in HiPIMS (lower row, d-f) with various  $C_2H_2$  flow rates: (a, d) 10 sccm, (b, e) 14 sccm and (c, f) 16 sccm.

The surface morphologies of the films deposited in both DC and HiPIMS exhibit uniformly distributed granular structure. As the  $C_2H_2$  flow rate increases, the average size of these granules increases, and the surface morphology gradually becomes rough. Moreover, the roughness of the HiPIMS deposited film is higher than that of the DC deposited film, which is caused by the columnar growth of the HiPIMS deposited film that naturally results in a rough surface. Besides, the rougher surface of the HiPIMS deposited film also stems from the higher substrate temperature, a by-product of higher bombardment energy, of the HiPIMS process. The

higher substrate temperature adjusts the diffusion process of condensed atoms at the growing interface and forces them to aggregate into larger-sized clusters, thereby creating a rougher surface.

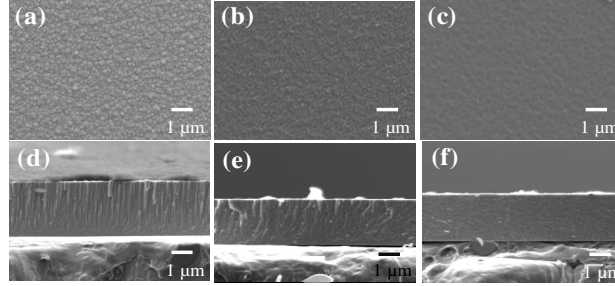


Figure 3. SEM micrographs of top surfaces (a-c) and of cross-sections (d-f) of HiPIMS deposited TaC/a-C:H films at 16 sccm  $C_2H_2$  with different substrate bias: (a) floating, (b) -50 V, (c) -100 V

Take the films deposited at 16 sccm  $C_2H_2$  as an example, the SEM micrographs of TaC/a-C:H films with different substrate biases prepared in HiPIMS are presented in Fig. 3. At the substrate bias of -50 V, the columnar structure previously seen is interrupted and replaced by a denser and less structured morphology (see Fig. 3(e)) and then, as the bias voltage increases to -100 V, the columnar growth disappears completely, evolving to a glassy morphology (Fig. 3(f)). Moreover, the top surface tends to be smooth with the substrate bias and exhibits a character of slight etching at -100V bias. These denser cross-sections and smoother surfaces are due to the high kinetic energy of ion bombardment, which impacts a few atomic layers beneath the growing interface and delivers sufficient mobility for atomic rearrangement.

Fig. 4 shows a series of X-ray diffractograms for TaC/a-C:H films with different  $C_2H_2$  flow rate. The left and right sides represent the diffraction spectra of DC and HiPIMS deposited films, respectively. For the DC film deposited at 10 sccm  $C_2H_2$ , the diffraction peaks observed at  $2\theta \approx 42.5^\circ$  and  $44.5^\circ$  are ascribed to (002) and (101) of the hexagonal  $Ta_2C$  phase. As the  $C_2H_2$  flow rate increases from 12 to 14 sccm, a strong peak at  $2\theta \approx 40.65^\circ$  and a very weak peak at  $2\theta \approx 47.29^\circ$  present, which are assigned to (111) and (200) of the fcc TaC phase. It indicates that the DC deposited films at 12 and 14 sccm exhibit the (111) preferred orientation. As

the  $C_2H_2$  flow rate increases to 16 and 18 sccm, the diffraction peaks at  $2\theta \approx 40.65^\circ$ ,  $47.29^\circ$  and  $69.12^\circ$  coexist, corresponding to (111), (200) and (220) of fcc TaC.

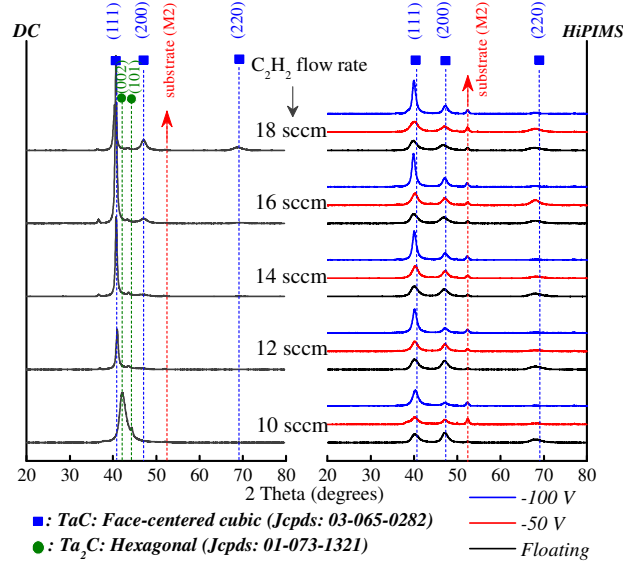


Figure 4. X-ray diffractograms of TaC/a-C:H films deposited in DC (left) and HiPIMS (right).

For HiPIMS films (without substrate bias) deposited with  $C_2H_2$  flow rate from 10 to 18 sccm, the diffraction peaks distribute at  $2\theta \approx 40.65^\circ$ ,  $47.29^\circ$  and  $69.12^\circ$  corresponding to (111), (200) and (220) lattice planes of fcc TaC, respectively. With increasing  $C_2H_2$  flow rate, these diffraction peaks exhibit similar intensities with a slight left shift. Generally, the shift of the diffraction peak toward a lower angle is related to lattice expansion and/or compressive stress. From Fig. 8(b), the compressive stress of the HiPIMS (floating) deposited films (black line with ball) remains almost unchanged. Hence, it can be inferred that the left shift of the peak position derives from lattice expansion caused by the stoichiometric change of TaC grains [41][42]. As the substrate bias increases in HiPIMS, the full width at half maximum (FWHM) of (111) peak narrows monotonically, accompanied by an increase in intensity. It corresponds to the coarsening of the microstructure, provided by the enhanced substrate temperature due to the high energy ion bombardment effect of the substrate bias.

The mean grain size of TaC/a-C:H films as a function of the  $C_2H_2$  flow rate under different deposition conditions are shown in Fig. 5. It is calculated from the Scherrer formula, where the total broadening of the

FWHM is attributed to the grain size while the strain broadening is ignored. It can be seen that the grain size of the HiPIMS deposited film is smaller than that of the DC deposited film at each  $C_2H_2$  flow rate. This is caused by the higher ionization rate induced by HiPIMS plasma and the higher amorphous carbon content in HiPIMS deposited films. On the one hand, the higher ionization rate of the HiPIMS plasma will interrupt the growth of TaC grains and thus force the newly arrived TaC-forming species to renucleate. On the other hand, the higher content of amorphous carbon is more effective in inhibiting grain growth. Therefore, the grain size of the HiPIMS deposited film is easily refined. For the grains that gradually coarsen with increasing substrate bias in HiPIMS, the fundamental driving mechanism is the enhanced ion bombardment effect, since the elevated ion velocity and energy serve the same role as substrate heating. Furthermore, the less amorphous carbon content with the substrate bias provides a weaker growth-inhibiting effect on TaC grains.

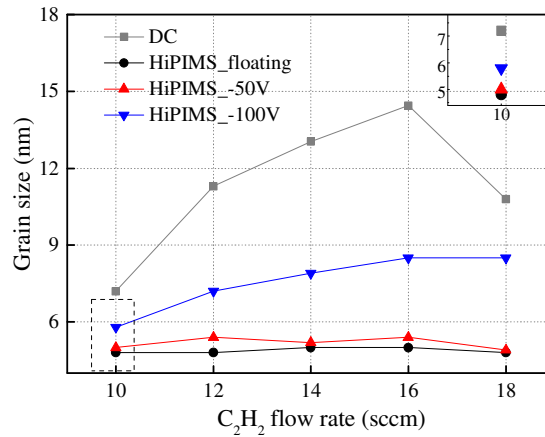


Figure 5. The grain size of TaC/a-C:H films deposited in different conditions with various  $C_2H_2$  flow rates.

Apart from the overall comparison of the grain size under different deposition conditions, the evolution of grain size with the  $C_2H_2$  flow rate also shows deposition condition-dependence. For DC deposited films, the grain size first increases from 7.2 to 14.5 nm, and then decreases to 10.9 nm, with a turning point at 16 sccm  $C_2H_2$  flow rate. From 10 to 16 sccm  $C_2H_2$  flow rate, the increase in carbon source provides a favorable growth condition for the phase of tantalum carbide. The TaC grains are therefore gradually coarsened and reach a maximum size of 14.5 nm. As the further increasing  $C_2H_2$  flow rate exceeds 16 sccm, the amorphous carbon

matrix surrounding the TaC grains reaches an appropriate amount capable of isolating TaC grains, thereby hindering the growth of the TaC grains through its encapsulation role. Similar evolution of grain refinement with increasing carbon content in nc-MeC/a-C:H (Me stands for transition metal) films has been reported in [43][44].

For the films deposited in HiPIMS with floating substrate and -50 V bias, the grain size remains unchanged, which is consistent with the results of [34][36]. It is known that the evolution of TaC grain in TaC/a-C:H film is governed by the competition between the grain growth and the hindering effect of the amorphous carbon matrix. Since the grain size is finer and the content of amorphous carbon is higher in the HiPIMS deposited film (indicated by XPS) compared to those in DC deposited film, the hindering effect of sufficient amorphous carbon content acted on the growing grains is more pronounced in HiPIMS deposited films. As a result, the grain coarsening with increasing C<sub>2</sub>H<sub>2</sub> flow rate from 10 to 16 sccm (as occurred in DC deposited film) is suppressed to some extent, the grain size remains unchanged in this interval. At the C<sub>2</sub>H<sub>2</sub> flow rate of 18 sccm, HiPIMS film still contains a higher content of amorphous carbon and finer grains than those of DC deposited film, which suggests a stronger inhibition of amorphous carbon on the grain growth. However, the grains were not suppressed at 18 sccm C<sub>2</sub>H<sub>2</sub> flow rate. The grains that are not inhibited here are explained by the higher bombardment energy of the HiPIMS plasma which enhances the reactivity of Ta species with carbon at growing interface and thus prompts the growth of TaC grains. Consequently, it can be stated that for the films deposited in HiPIMS with floating and -50 V bias, the constant trend of grain size (from 10 to 18 sccm C<sub>2</sub>H<sub>2</sub>) is the almost balanced result of the competition between the hindering effect of amorphous carbon and growth of grains.

For films deposited in HiPIMS with -100 V substrate bias, the grain size is neither reduced nor kept constant but is gradually coarsened in the range of 5.8 to 8.4 nm (from 10 to 18 sccm C<sub>2</sub>H<sub>2</sub> flow rate). It is attributed to two aspects. Firstly, in the case of HiPIMS operating at high substrate bias, the ion bombardment effect dominates the chemical bonding state of the film, manifesting as a reduction in amorphous carbon content. The sealing and suppressing effect of less amorphous carbon matrix on the TaC grain growth is thus weakened. Secondly, the bombardment energy of film-forming species is strong. Under the condition of -100 V substrate bias, the bombardment energy of species is not only derived from the energy delivered by the sputtering process on the target surface, but also from the high potential of the biased substrate. After the

film-forming species experience collisions and lose partial energy, they can regain energy from the potential of the biased substrate due to the high ionization rate of the HiPIMS plasma. Therefore, the degree of reaction of Ta species reaching the substrate with carbon is very high at the growing interface, which is conducive to the growth of TaC grains. The synergy of these two aspects promotes grain growth to be superior in the aforementioned competition and thus the grain is gradually coarsened. This growing grain size with increasing carbon content is consistent with the results of [38], in which the used deposition condition is HiPIMS with -150 V substrate bias.

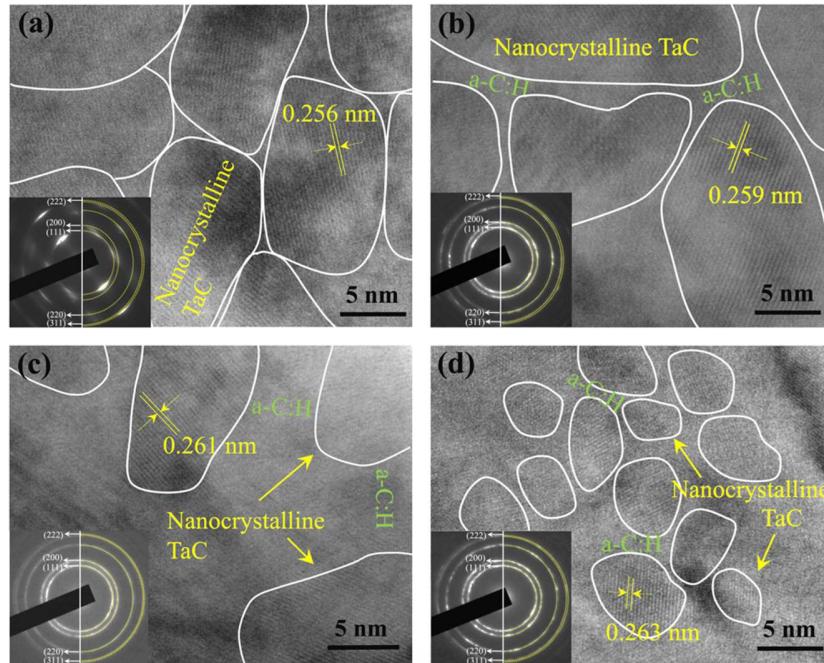


Figure 6. The HRTEM images and corresponding SAED patterns of TaC/a-C:H films deposited in DC with (a) 12 sccm (b) 16 sccm and (c) 18 sccm and in HiPIMS with (d) 16 sccm  $C_2H_2$  flow rates.

The microstructures of four representative TaC/a-C:H films, deposited in DC with 12, 16 and 18 sccm  $C_2H_2$  flow rates and in HiPIMS with 16 sccm  $C_2H_2$  flow rate, are also investigated by high-resolution TEM and the corresponding selected area electron diffraction (SAED), shown in Fig. 6. The typical nanocomposite structure composed of TaC grains dispersed in the amorphous carbon matrix is clearly exhibited at all TaC/a-C:H films.

For the film deposited in DC with 12 sccm (Fig. 6(a)), the grain size is about 12 nm and the inter-planar spacing ( $d$ ) is measured to be 0.256 nm. The crystalline TaC grains are not completely separated by the amorphous carbon matrix, presenting many interconnected grain boundaries. In Fig. 6(b), the film deposited at 16 sccm exhibits a large grain size of 17 nm while the  $d$  of TaC grain is 0.259 nm. The TaC grains are well separated by amorphous carbon matrix, and the width of mean grain separation is about 1.5 nm. As the  $C_2H_2$  flow rate rises to 18 sccm (Fig. 6(c)), the grain size decreases and more amorphous carbon matrix is observed. The  $d$  increases to 0.261 nm, while the width of mean grain separation increases to ~4 nm. With the  $C_2H_2$  flow rate increases in DC condition, the crystallinity of the film degrades, accompanied by the widening of the mean grain separation. This trend can also be confirmed by the corresponding SAED patterns. For the film deposited in HiPIMS with 16 sccm (Fig. 6(d)), it can be observed that nanocrystalline TaC (4 nm) is uniformly dispersed in the amorphous carbon matrix, with a mean grain separation of ~1 nm. The inter-planar spacing expands to 0.263 nm, corresponding to the higher stoichiometric ratio of TaC grains.

### 3.3 Mechanical properties

The hardness  $H$  and Young's modulus  $E$  of the TaC/a-C:H films with various  $C_2H_2$  flow rates are plotted in Fig. 7. The hardness and Young's modulus of TaC/a-C:H films prepared in DC and HiPIMS (without substrate bias) have the same evolutionary trend. It can be seen from Fig. 7 that as the  $C_2H_2$  flow rate increases from 10 to 16 sccm,  $H$  and  $E$  increase correspondingly. The values of hardness and Young's modulus increase from 25.8 and 298 to 35.0 GPa and 385 GPa for DC deposited film, while for HiPIMS deposited film, they increase from 32.7 and 369 to 40.6 GPa and 427 GPa, respectively. Both  $H$  and  $E$  reach maximum values at 16 sccm of  $C_2H_2$ . Once the  $C_2H_2$  flow rate further increases to 18 sccm, the evolutions of  $H$  and  $E$  reverse and begin to decrease.

It is known well that for carbon-based nanocomposite films, the grain size, mean grain separation, stoichiometric ratio, matrix properties, and growth morphology are important factors in determining the mechanical properties of the film. For TaC/a-C:H films deposited in DC, the growth morphology (indicated by the SEM) is very similar regardless of the  $C_2H_2$  flow rate. At the same time, the ratio  $sp^3/sp^2$ -C, which acts to harden the carbon matrix, gradually decreases since  $sp^2$ -C increases and  $sp^3$ -C floats randomly in a small range (obtained from XPS) as the  $C_2H_2$  flow rate increases. It can therefore be stated that the two factors of

morphology and matrix properties ( $sp^3/sp^2$ ) do not contribute to the mechanical properties of the DC deposited films. With the  $C_2H_2$  flow rate increases from 12 to 18 sccm, the grain size of DC deposited film first increases and then decreases. Note that the film deposited at 10 sccm  $C_2H_2$  exhibits the  $Ta_2C$  phase. Here we only consider the influence of the TaC phase. According to the Hall-Petch relation, this trend of grain size suggests that the hardness first decrease and then increase, which is contrary to what we observed. However, for the carbon-based nanocomposite film, the increased amorphous carbon content causes the grains to be gradually separated despite the continued increase in grain size, which is confirmed by Fig. 6(a-c). Therefore, the film hardness gradually rises as the  $C_2H_2$  flow rate increases from 12 to 16 sccm, since the narrow mean grain separation will cause dislocation motion to be suppressed. At 16 sccm  $C_2H_2$  flow rate, the width of mean grain separation is about 1.5 nm while the TaC grain size is about 17 nm (indicated by HRTEM images). This narrow mean grain separation can effectively restrict the deformation under applied load caused by dislocation movement and decrease cracks propagation [36][41], thereby leading to the optimal hardness. As the  $C_2H_2$  flow rate further reaches 18 sccm, the grain size drops while the amorphous carbon content continues to increase. The mean grain separation is thus widened significantly to  $\sim 4$  nm, as displayed in Fig. 6(c). Too wide grain separation, filled by the amorphous carbon matrix, not only promotes the influence of the amorphous carbon phase on the film properties but also provides more space for nano-crack initiation and propagation, therefore causing a decrease in hardness [45].

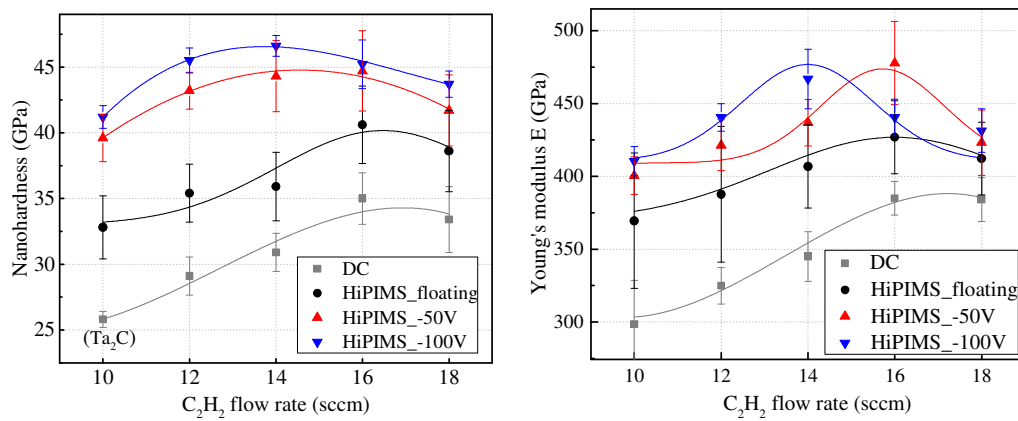


Figure 7. Hardness H and Young's modulus E of TaC/a-C:H films with various  $C_2H_2$  flow rate.

Besides, as the  $C_2H_2$  flow rate increases from 12 to 18 sccm, the stoichiometric ratio of DC deposited film increases from 0.5 to 0.69. It is known that, apart from the factors discussed above, the mechanical properties of fcc Ta-C system also derive from the electronic structure and bonding state of the mixed metal-covalent character. Carbon vacancies are responsible for this electronic structure and can be used to tune Fermi level which plays a leading role in bond strength. Therefore, appropriate content of carbon vacancies, expressed as a substoichiometric ratio, is favorable for obtaining the highest hardness [2][3]. Riedl, H. *et al.* [3] reported that for the single-phase fcc structured  $TaC_x$  coatings, the low-carbon  $TaC_{0.78}$  film exhibited the highest hardness. When  $x$  exceeds 0.78, the hardness begins to decrease. Hong, Q. *et al.* [46] demonstrated through electronic structure calculation that the maximum hardness and melting temperature can be obtained when  $x \leq 0.85$  of the  $TaC_x$  system. For the TaC/a-C:H films in our case, although XPS technology being used to obtain stoichiometric ratio has measurement errors, we suspect that  $x=0.69$  is still less than the critical value of the substoichiometric ratio for driving maximum hardness. Therefore, the increase in the stoichiometric ratio in DC deposited films from 12 to 18 sccm continuously increases the hardness. The reduced hardness at 18 sccm is dominated by the too wide mean grain separation, and here the stoichiometric hardening effect may be offset.

For HiPIMS (without substrate bias) deposited films, as the  $C_2H_2$  flow rate increases, the trends of morphology and ratio  $sp^3/sp^2$  -C are similar to those of DC deposited films. It means that for HiPIMS deposited films, these two factors are also independent of the evolution of mechanical properties, as they did for DC deposited films. In addition, as the  $C_2H_2$  flow rate increases, the grains that remain constant in size are separated by the growing content of the amorphous carbon matrix, and the separation is getting larger. From HRTEM image (Fig. 6(d)), the mean grain separation reaches about 1 nm as the  $C_2H_2$  flow rate up to 16 sccm. The gradually formed grain separation will hinder the dislocation operation and induce the grain incoherence strains, which can enhance the resistance to plastic deformation [50]. Therefore, the film hardness increases from 10 sccm and achieves maximum at 16 sccm. However, at 18 sccm  $C_2H_2$  flow rate, the larger separation may provide sufficient space to make grain slip and rotate easier, thereby worsening the film hardness. Besides, the stoichiometric ratio of HiPIMS deposited film increases from 0.65 to 0.78 as the  $C_2H_2$  flow rate increases from 10 to 18 sccm. It is considered that this increase in stoichiometric ratio favors the rise of hardness in the segment of 10 to 18 sccm. Therefore, the observed reduced hardness at 18 sccm may be ultimately determined

by the result of the competition between stoichiometric hardening and softening of mean grain separation (excessively wide), which is similar to that in DC deposited films. In summary, it can be concluded that the evolutions of the hardness of DC and HiPIMS (without substrate bias) deposited films are dominated by two factors, mean grain separation and stoichiometric ratio of TaC grain.

Comparing the mechanical properties of DC and HiPIMS deposited films, at all C<sub>2</sub>H<sub>2</sub> flow rates, the hardness and Young's modulus of HiPIMS deposited films are higher than those of DC deposited films. It is attributed to the finer grain size (*i.e.*, the high volume of grain boundaries), higher stoichiometric ratio, and greater compressive stress (as indicated by Fig. 8(b)) of the HiPIMS deposited films supported by the HiPIMS plasma. These HiPIMS plasma-designed features of the film on the nanoscale level can prevent the operation of dislocations and upgrade the mechanical properties.

As the substrate bias increases in HiPIMS, the hardness of TaC/a-C:H film increases at each C<sub>2</sub>H<sub>2</sub> flow rate. The compressive stress also increases with the substrate bias, as shown in Fig. 8. It can be seen that the hardness increases dramatically in the segment of floating to -50 V bias and increases slightly in the segment of -50 V to -100 V bias. Interestingly, this growth ratio of hardness in different bias segment is opposite to that of compressive stress, which rises slightly in the range of floating to -50 V and increases considerably in the range of -50 V to -100 V. Although it is widely held that higher compressive stress in the film gives rise to higher hardness, the compressive stress hardening here is not the main driving force for increased hardness. Moreover, the content of the amorphous carbon matrix decreases while the grains coarsen as the substrate bias increases. That is, under the same C<sub>2</sub>H<sub>2</sub> flow rate, the mean grain separation is reduced with the application of the substrate bias. It is indicative of lower hardness, as opposed to the measured hardness trend. Besides, the sp<sup>3</sup>-C content decreases as the substrate bias increases. The change in matrix property thus does not contribute to the enhanced hardness. Based on the above discussion, by excluding these known factors for improving film hardness, one can speculate that the enhanced film hardness is related to the increase of the stoichiometric ratio of TaC grains. The correlation between stoichiometry and hardness in TaC nanocomposites has been demonstrated by [51][52][3]. It was observed in [51][52] that the hardness of the carbides of group VB metals, such as NbC<sub>x</sub> and TaC<sub>x</sub>, increases accordingly and reproducibly as the stoichiometric ratio increases, and reaches a maximum at the stoichiometric ratio of 0.88. H. Riedl *et al.* [3] demonstrated that for TaC films, in

the regime where the stoichiometric ratio is below 0.78, the film hardens as the stoichiometric ratio increases. For the TaC/a-C:H films in our work, the stoichiometric ratio of TaC grain increases with the substrate bias, confirmed by the calculation of XPS. Taking the films deposited at 12 sccm  $C_2H_2$  as an example, the stoichiometric ratio rises from 0.7 to 0.73, which is consistent with the increase in hardness. In addition, the denser morphology with the substrate bias also partially contributes to the increased hardness.

When we observe the overall trend of film hardness as a function of the  $C_2H_2$  flow rate under the three bias modes of HiPIMS (in Fig. 7), the maximum hardness gradually shifts to the left with the substrate bias increases from floating to -100 V and occurs at 14 sccm with -100 V bias. Comparing the TaC/a-C:H films deposited at 14 and 16 sccm  $C_2H_2$  under the bias of -100 V, their morphologies are similar in density and the film deposited at 16 sccm has higher compressive stress (which indicates a higher hardness). Meanwhile, the stoichiometric ratio of the film deposited at 14 sccm is 0.77 and at 16 sccm is 0.81 (shown in Table 1). It can thus be speculated that the lower hardness of the film deposited at 16 sccm is caused by the stoichiometric ratio of 0.81, which may exceed the threshold for determining the maximum hardness in the Ta-C film. Therefore, in the case of the substrate bias, the mean grain separation and compressive stress are subordinate to the stoichiometric ratio and morphology with regards to influencing film hardness. Moreover, the substoichiometric ratio for obtaining the optimal hardness appears at  $x \approx 0.77$ , which is close to the threshold observed in [3].

The mechanical behavior of TaC/a-C:H film is also characterized by the ratio H/E, which reflects the toughness of the film characterizing the film's ability to absorb energy and plastically deform without fracturing [47][48]. It is well known that hard nanocomposite film with enhanced toughness is desirable because it greatly contributes to the optimization of tribological performance. However, hard nanocomposite films are considered to lack toughness [49] since hardness and toughness are mutually coupled and there is a contradiction relation between them [47]. In the present work, the H/E ratios of the TaC/a-C:H films as a function of the  $C_2H_2$  flow rate are shown in Fig. 8(a). For DC and HiPIMS (without substrate bias) deposited films, their H/E ratios exhibit a trend consistent with the evolution of hardness. Moreover, the H/E ratios of HiPIMS deposited films are greater than those of DC deposited films in all  $C_2H_2$  flow rates. For the films deposited in HiPIMS with substrate bias, H/E ratio is substantially promoted with increasing bias value at each  $C_2H_2$  flow rate. It stems

from the large increase in hardness and the slight rise in Young's modulus with the substrate bias. These results in Fig. 8 indicate that the TaC/a-C:H films deposited by HiPIMS possess higher toughness.

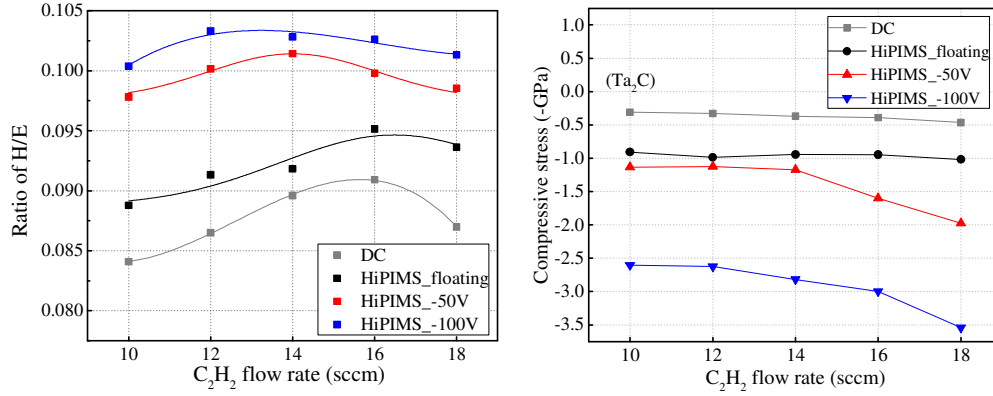


Figure 8. Ratio H/E and compressive stress of TaC/a-C:H films as a function of the C<sub>2</sub>H<sub>2</sub> flow rate.

The improved toughness in HiPIMS conditions is interpreted as the random orientation of the grains (indicated via XRD), smaller grain size, and higher content of amorphous carbon of the HiPIMS deposited films. The random orientation (i.e., high angle grain boundaries) can minimize the grain incoherence strain and promote the grain boundary sliding in the nanocomposite film [50]. The smaller grain size creates a large volume of grain boundaries and diminishes the size of the initial crack. The higher content of amorphous carbon can absorb the elastic energy released under load due to its relative Physico-chemical inertness. The synergy of these factors are capable of (i) releasing the strain by easier grain boundary sliding under the load exceeding elastic strength, and (ii) terminating the propagation of cracks through the deflection effect at high volume grain boundaries and the absorption of strain energy within amorphous carbon matrix. Both of them are responsible for improving toughness, thus the higher toughness is achieved in HiPIMS deposited films. Generally, the toughness can be improved in two ways, one is by adding a second metal element as the ductile phase, and the other is by regulating the nanostructure (grain size and distribution of amorphous carbon). However, despite the means of toughening, it is still not easy to achieve toughening while holding high hardness due to the high requirements for precise adjustment of the nanocomposite structure. Fortunately, in the present work, HiPIMS

deposition (including floating and biased substrate) is indicated to be a promising synthetic method for effectively regulating nanocomposite structures to enhance toughness.

### 3.4 Tribological behavior

The dynamic friction curves of TaC/a-C:H films deposited in DC and HiPIMS as a function of sliding laps are shown in Fig. 9. Among them, the HiPIMS TaC/a-C:H films deposited at 16 sccm  $C_2H_2$  are chosen as a representative to reveal the effect of substrate bias on the friction behavior. Furthermore, Fig. 10 summarizes the friction coefficient values and wear rates of all TaC/a-C:H films prepared in DC and HiPIMS.

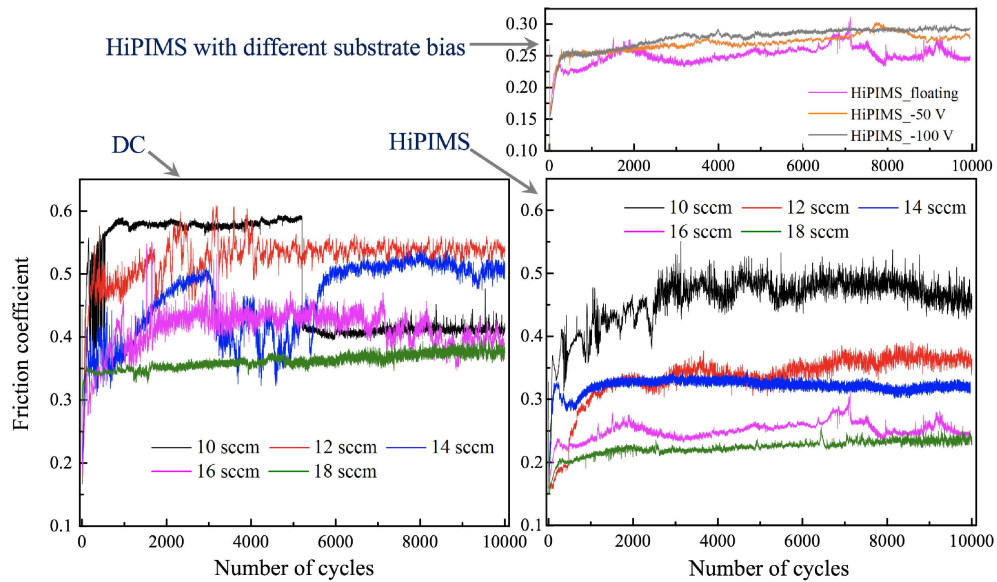


Figure 9. Friction coefficients of TaC/a-C:H films deposited in different conditions as a function of sliding cycle: (a) DC, (b) HiPIMS with floating substrate, (c) HiPIMS with different substrate bias (at 16 sccm  $C_2H_2$ ).

For the friction coefficient, as the  $C_2H_2$  flow rate increases from 10 to 18 sccm, its value decreases from 0.6 to 0.37 for DC deposited films and decreases from 0.47 to 0.23 for HiPIMS (without bias) deposited films. Meanwhile, the features of the dynamic friction curves evolve from dramatic fluctuations (i.e., with a large number of burrs) to minor fluctuations with increasing  $C_2H_2$  flow rate in both DC and HiPIMS. Note that for the DC TaC/a-C:H film deposited at 10 sccm, the friction curve suddenly drops to 0.42 (approximating the

friction coefficient of WC ball sliding on substrate M2) after 5200 sliding cycles, which is due to the film being completely worn through. The friction coefficient of M2 at about 0.4 has also been reported in [53][54]. Both trends of reduced friction coefficient and smoothed friction curve are attributed to the increase in  $sp^2$ -C content with the increase of  $C_2H_2$  flow rate. As the  $C_2H_2$  flow rate increases to 18 sccm, the  $sp^2$ -C content reaches 20.6 at.% and 30.6 at.% in the films deposited in DC and HiPIMS, corresponding to the minimum friction coefficients of 0.37 and 0.23, respectively. Moreover, the friction coefficients of HiPIMS deposited films are lower than those of DC deposited films. The friction curves of HiPIMS deposited films exhibit slighter fluctuations compared to those of DC deposited films at all  $C_2H_2$  flow rates. These better friction performances are determined by the higher  $sp^2$ -C content in the HiPIMS deposited films. Since the  $sp^2$ -C phase enhances the formation of an easily sheared graphitic tribolayer, the film with higher content of  $sp^2$ -C exhibits superior friction behavior.

The application of the substrate bias from floating to -100 V in HiPIMS results in an increase in friction coefficient at all  $C_2H_2$  flow rates. It is caused by the decrease in  $sp^2$ -C content as the substrate bias increases (evidenced by XPS), which weakens the self-lubricating effect on the film surface. Such a friction behavior developed with the substrate bias is consistent with the literature [55][56][12]. It is worth noting that compared with the DC deposited films, the films deposited in HiPIMS with -100 V bias possess lower  $sp^2$ -C contents (see Table 1) but exhibit lower friction coefficients. Moreover, the dynamic friction curve of the film deposited in HiPIMS with -100 V is smoother, that is, the fluctuations thereon become invisible. They are explained by the higher hardness and toughness of the films under biased substrate conditions. Since the better mechanical properties of the film can weaken the plastic plough and reduce the level of mechanical interlocking between the film surface and the WC ball, less significant abrasive wear and less wear debris are generated, thereby ultimately reducing the value of the friction coefficient and smoothing the friction curve. To sum up, combining the friction coefficients of the films under different deposition conditions, it is concluded that the friction coefficient of TaC/a-C:H film is controlled by the synergy of  $sp^2$ -C content and mechanical properties.

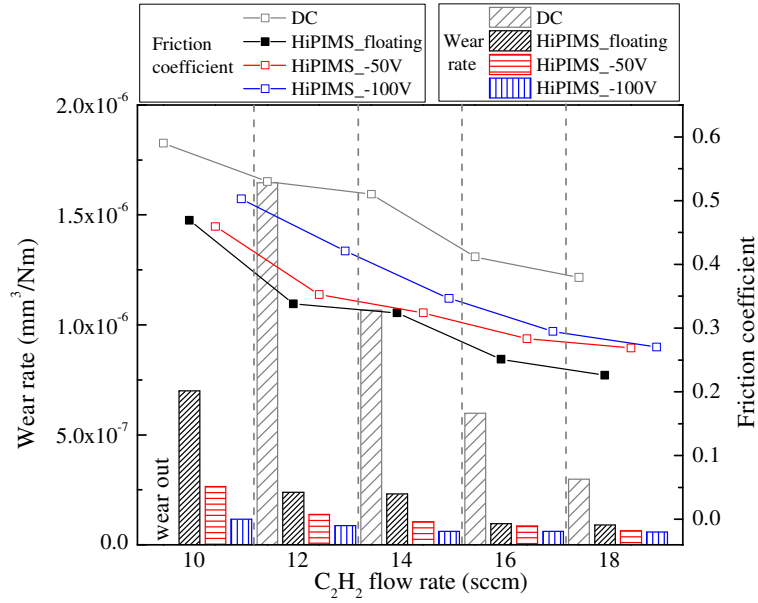


Figure 10. Friction coefficient (lines) and wear rate (columns) of TaC/a-C:H films as a function of the C<sub>2</sub>H<sub>2</sub> flow rate.

For the wear rate, shown as columns in Fig. 10, it exhibits a tendency consistent with that of friction coefficient in DC and HiPIMS (without substrate bias). As the C<sub>2</sub>H<sub>2</sub> flow rate increases from 10 to 18 sccm, it gradually decreases in the range of  $1.7 \times 10^{-6} \rightarrow 2.6 \times 10^{-7} \text{ mm}^3/\text{N}$  for DC films and in the range of  $7.0 \times 10^{-7} \rightarrow 8.9 \times 10^{-8} \text{ mm}^3/\text{Nm}$  for HiPIMS films. Note that the wear rate of the DC film deposited at 10 sccm C<sub>2</sub>H<sub>2</sub> is not shown in Fig. 10 since this film is completely worn through. It can also be observed that the application of substrate bias in HiPIMS can further reduce the wear rate, contrary to its effect on the friction coefficient. For a more detailed analysis of the wear behavior, Fig. 11 exhibits the SEM images of the wear tracks on both DC and HiPIMS deposited films. Moreover, the HiPIMS films deposited under 12 sccm C<sub>2</sub>H<sub>2</sub> with different substrate biases are taken as a representative case to analyze the influence of the substrate bias on the wear behavior. The evolution of the top view and cross profile of the wear track is shown in Fig. 12.

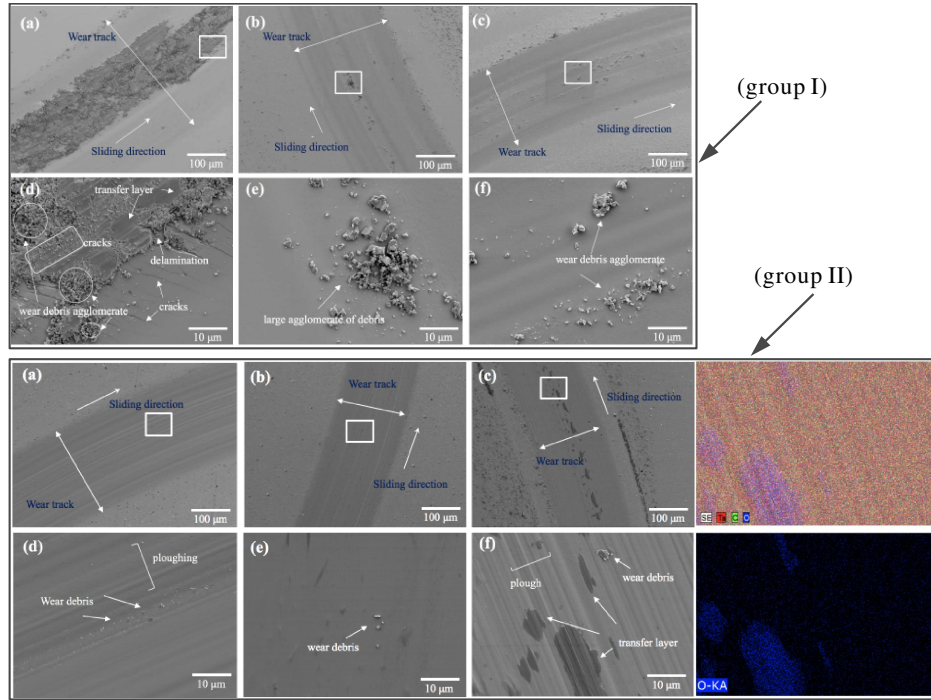


Figure 11. Wear tracks of TaC/a-C:H films deposited in DC (group I) and HiPIMS (group II). In both groups, (a), (b) and (c) represent the films prepared at 12 sccm, 16 sccm and 18 sccm  $C_2H_2$ , where (d), (e), (f) are magnified views of the white squared regions in (a), (b), (c). The EDS maps of the subgraph (f) are displayed on the right side of group II.

From Fig. 11, it can be observed that in both DC and HiPIMS (without substrate bias), the wear track of the film becomes narrower and shallower as the  $C_2H_2$  flow rate increases, which is consistent with the evolution of friction coefficient. At 12 sccm  $C_2H_2$  flow rate, the wear track of the film deposited in DC is locally damaged, showing the obvious delamination, accumulated wear debris, grooves and cracks at the boundary of the film breakage. However, there are no detected failures, agglomerated debris and cracks on the wear track of the HiPIMS deposited film at the same  $C_2H_2$  flow rate. Meanwhile, distinct grooves parallel to the sliding direction are observed on this wear track through the corresponding enlarged image. These results of the DC and HiPIMS films deposited at 12 sccm  $C_2H_2$  stem from poor hardness and toughness, as well as severely insufficient amorphous carbon content. The lack of amorphous carbon content causes a large shear sliding resistance between the counterpart ball and the film surface. The poor hardness leads to a larger sliding contact surface

(between the counterpart ball and the film) and a deeper penetration distance under applied load, which thus generates a wider wear track and higher wear rate. Also, poor hardness has less resistance against abrasion (of wear debris) during the test, resulting in a pronounced groove distribution [47][57]. The poor toughness does not effectively prevent crack propagation and then causes delamination and failure to take place after sliding multiple times. Therefore, the higher wear rate (of HiPIMS film) and local failure (of DC film) appear at 12 sccm  $C_2H_2$  flow rate. Besides, these severe wear and local failure of the films deposited at 12 sccm  $C_2H_2$  are another reason for the high friction coefficient value and the dramatic fluctuation of the friction curve in addition to the low  $sp^2$ -C content.

As the  $C_2H_2$  flow rate increases to 16 sccm, the wear tracks become smoother and narrower and the grooves become shallower in DC and HiPIMS. It indicates improved wear resistance and is attributed to the continued increase in hardness, toughness and  $sp^2$ -C content. Moreover, compared to DC deposited films, less debris and narrower wear track are observed in HiPIMS deposited films. As the  $C_2H_2$  flow rate further increases to 18 sccm, the wear tracks are slightly narrower in both DC and HiPIMS. The accumulated debris on the wear track of the DC deposited film is greatly reduced. However, on the wear track of the HiPIMS deposited film, the grooves which are almost invisible at 16 sccm become deeper again, and the distinct tribolayer appears revealed by EDS maps. The reappearance and deepening of the groove is due to the decrease in hardness after the  $C_2H_2$  flow rate exceeds 16 sccm. Since the wear debris acts as grinding particles and abrades the film surface during the test process, the impaired hardness weakens the resistance of the film against abrasion under continual periodic load, thereby deepening the groove again. It is worth noting that although the hardness is reduced and the groove distribution is deepened, the wear rate of the film deposited at 18 sccm  $C_2H_2$  does not deteriorate rather than continues to decrease with increasing  $C_2H_2$  flow rate. This is due to the lowest friction coefficient and the initial formation of the tribolayer, which reduces the sliding resistance and acts as a protective layer to reduce the direct contact between the counterpart ball and the film surface to some extent, thereby contributing to the diminution of wear rate.

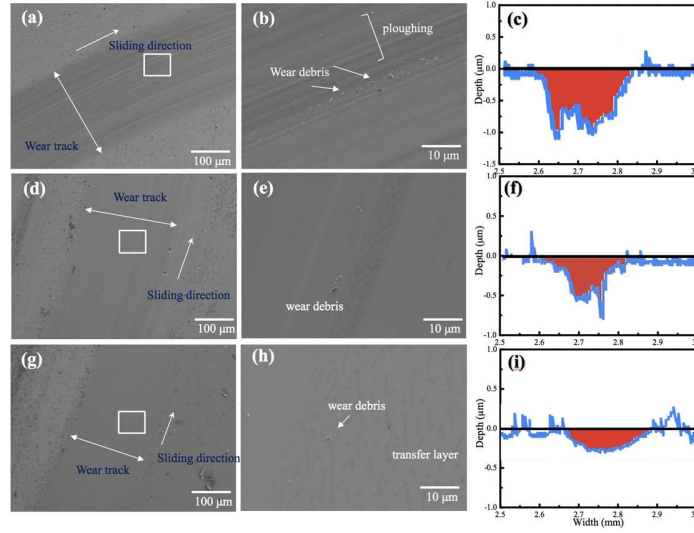


Figure 12. SEM images and cross profiles of wear tracks for HiPIMS TaC/a-C:H films deposited at 12 sccm  $C_2H_2$  flow rate with different substrate bias: (a-c) floating, (b-f) -50 V, (g-i) -100 V.

It can be seen from Fig. 12 that as the substrate bias increases, the wear track of the film deposited at 12 sccm  $C_2H_2$  flow rate becomes narrower and smoother significantly. It is contrary to the evolution of the friction coefficient. The film deposited under the floating substrate is characterized by the obvious plowing grooves and wear debris, confirmed by the corresponding enlarged SEM image and cross profile of the wear track. With the substrate bias increases to -100 V, the wear track becomes narrower and the wear debris decreases. Meanwhile, it can be observed from the enlarged SEM image and cross profile that the surface of the wear track becomes very smooth. These results suggest a higher resistance against abrasion as the substrate bias increases, which is supported by the increased hardness, toughness and compressive stress. With the substrate bias rises from floating to -50 V and then to -100 V, the hardness of the film deposited at 12 sccm  $C_2H_2$  flow rate increases from 35.4 to 43.2 and then to 45.5 GPa, while the compressive stress increases from -0.98 to -1.12 and then to -2.61 GPa. At the same time, the wear rate of the film (columns in Fig. 10) decreases linearly. Therefore, it can be stated that from the floating to -50 V bias, the reduction in wear rate is mainly due to the enhanced hardness, while in the range of -50 V to -100 V bias, it is attributed to the compressive stress. The contribution of compressive stress to the wear rate is consistent with that in [58].

In summary, the friction and wear performances of HiPIMS (with and without substrate bias) deposited films are superior to those of DC deposited films, exhibiting **less fluctuating friction curves**, smaller values of friction coefficient and wear rate, narrower and shallower wear tracks and less wear debris. There are three reasons for driving the better tribological performance of the HiPIMS deposited TaC/a-C:H films. First, HiPIMS discharge (**under floating and -50 V bias**) results in **a** higher content of sp<sup>2</sup>-C inside the film. Second, the higher bombardment energy of **the** HiPIMS plasma produces greater compressive stress, which helps to terminate crack nucleation and propagation and thus improves the wear resistance. Third, the hardness and toughness of **the** HiPIMS deposited films are higher. **They not only promote the reduction of friction coefficient and the improvement of wear resistance but also reduce the possibility of frictional interlocking during multiple sliding processes, which results in less wear debris and smoother friction curve.** Therefore, the rich sp<sup>2</sup>-C content and greater compressive stress, coupled with adequate hardness and toughness, qualify the HiPIMS deposited TaC/a-C: H film as an excellent candidate for tribological applications.

**Regarding the wear behavior of TaC/a-C:H films, there are two main factors.** On the one hand, under **the** DC and HiPIMS deposition conditions without substrate bias, the tribochemical nature of sp<sup>2</sup>-C content dominates the wear behavior (the higher the sp<sup>2</sup>-C content, the lower the wear rate), despite the decline in mechanical properties. This is because the presence of rich sp<sup>2</sup>-C facilitates easy shearing of the two sliding surfaces. Moreover, the specific interface (interphase boundary), provided by the relative Physico-chemical inert carbon matrix dispersed in the TaC grains, can dissipate and absorb the elastic energy released during the test and terminate the propagating cracks, which improves the wear resistance. **It is consistent with the wear behavior Nb- and Ti- carbide/amorphous carbon nanocomposite films reported in [8][14].** On the other hand, under HiPIMS with different substrate biases, the wear behavior of the film is controlled by mechanical properties and compressive stress. Although the content of sp<sup>2</sup>-C is lowered as the substrate bias increases, which causes shear sliding becomes difficult, the hardness, toughness and compressive stress are greatly increased. According to the delamination theory of wear proposed by Suh [59], the wear process consists of three stages: plastic deformation accumulation, crack nucleation and crack propagation. In the case of application of substrate bias, **higher hardness** (resisting plastic deformation) **and toughness** (enhancing

load-bearing capability) and **greater** compressive stress (preventing and slowing crack expansion) can enhance the wear resistance of the film. This trend is consistent with the result of [55].

### 3.5 Oxidation resistance

The oxidation resistance test was carried out for all TaC/a-C:H films. The results show that the oxidation resistance of the film remains almost unchanged with varying flow rates of  $C_2H_2$ . However, **the significant differences between the films prepared by different deposition conditions were observed**. In this section, the films deposited at 16 sccm  $C_2H_2$  flow rate are used as the representative to analyze the effect of deposition condition on the oxidation resistance of the film. The structural evolutions of **the** TaC/a-C:H films (at 16 sccm  $C_2H_2$  flow rate) with different annealing temperatures are illustrated in Fig. 13, where (a), (b) and (c) represent the results of the films deposited in DC, HiPIMS with floating substrate and HiPIMS with -100 V bias, respectively.

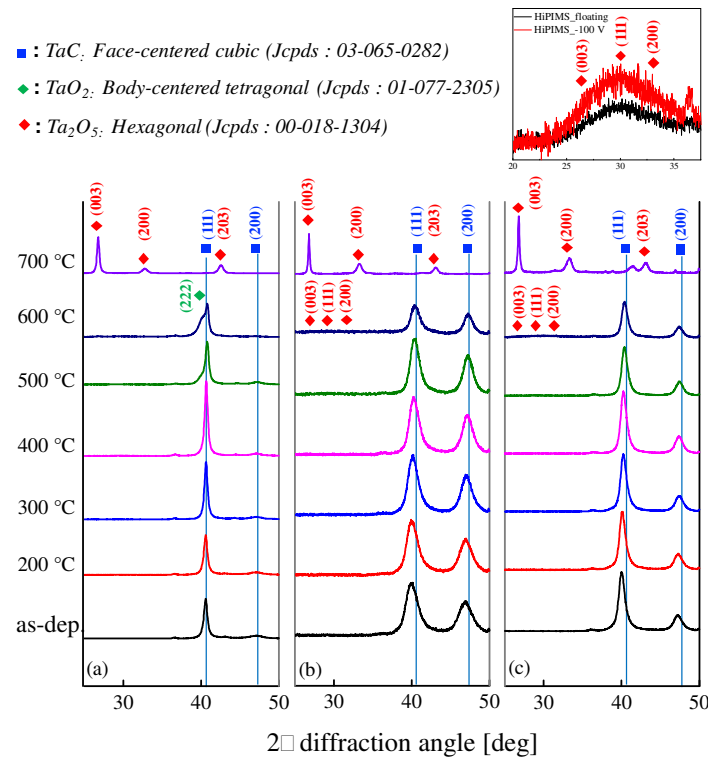


Figure 13. X-ray diffractograms of the TaC/a-C:H films deposited in different conditions as a function of annealing temperature: (a) DC, (b) HiPIMS with floating substrate, (c) HiPIMS with -100 V bias.

When the annealing temperature is below 400 °C, all TaC/a-C:H films perform well regardless of the deposition conditions. After annealing at 400 °C, the diffraction peaks become narrower and more intense for the film deposited in DC and HiPIMS with -100 V bias, which is explained by the slight coarsening of microstructure. After annealing at 500 °C, for the DC deposited film, the intensities of TaC peaks (111) and (200) begin to weaken, while the (222) peak of the TaO<sub>2</sub> phase begins to appear. For the films deposited in HiPIMS with -100 V bias, the decrease in the intensities of TaC peaks (111) and (200) are also observed, but no significant peaks of tantalum oxide are detected. It should be noted that for the film deposited in HiPIMS with floating substrate, no change in the intensity and width of the TaC peak is detected, indicating that the TaC phase of this film is the most stable.

After annealing at 600 °C, the two phases, TaC and TaO<sub>2</sub>, coexist in the DC deposited film. Moreover, the intensity of the TaO<sub>2</sub> peak reaches a level comparable to that of the (111) peak of TaC phase. It reflects a gradual phase transformation from TaC to TaO<sub>2</sub>. For the film deposited in HiPIMS with -100 V bias, three small peaks appear, identified as the (003), (111) and (200) planes of the Ta<sub>2</sub>O<sub>5</sub> phase, which confirms the beginning of oxidation. For the film deposited in HiPIMS with floating substrate, three Ta<sub>2</sub>O<sub>5</sub> peaks can also be observed, but their intensities are relatively weak (see the sub-figure in the upper right corner of Fig. 13). After annealing at 700 °C, no TaC peaks can be detected in all TaC/a-C:H films, indicating that the films are completely oxidized regardless of the deposition conditions. Besides, for the position of the XRD peak, the gradual right shift appears on all films as the annealing temperature rises from 200 °C to 600 °C, corresponding to the relaxation of compressive stress. Through this structural development at different oxidation temperatures, it is proved that the TaC/a-C:H film deposited in HiPIMS with floating substrate has stronger oxidation resistance compared to those deposited in DC and HiPIMS with -100 V bias. However, it is difficult to state the specific oxidation degree of the film based on the XRD diffractograms alone. For a more detailed comparison, the cross-sections of the films after annealing at 600 °C were analyzed by SEM and EDS, shown in Fig. 14.



For the film deposited in HiPIMS with floating substrate, the small-sized grains can be rapidly oxidized. The tantalum oxide layer can thus be formed at a faster rate on the film surface. This means that the rate of diameter reduction of the channels required for oxygen diffusion is faster, which is the key to limiting the rate of oxygen diffusion into the film. Meanwhile, the rapid formation of the oxide layer also consumes a large amount of oxygen (that will diffuse into the film), thereby slowing down the oxidation rate of the film. Therefore, the oxidation resistance of the film deposited in HiPIMS with floating substrate is higher. Besides, the oxidation resistance of film seems to be independent of the density of the film morphology. As our results show, the films prepared in the conditions of DC and HiPIMS with -100 V bias have denser morphologies (indicated by the SEM images in Fig. 2 and Fig. 3) but poorer oxidation resistance.

#### 4. Conclusion

TaC/a-C:H films were deposited utilizing HiPIMS (operated with three substrate bias: floating, -50 V and -100 V) and DC magnetron sputtering in the C<sub>2</sub>H<sub>2</sub>/argon mixed atmosphere. Analysis of the chemical bonding state, morphology, structure, mechanical and tribological properties, as well as oxidation resistance of the TaC/a-C:H films were conducted. The comparison between HiPIMS and DC (without substrate bias) deposited TaC/a-C:H films reveals that the properties of HiPIMS deposited films are superior to those of DC deposited ones, exhibiting higher hardness and toughness, lower friction coefficient and wear rate, and stronger oxidation resistance. It is attributed to the finer grains, higher stoichiometric ratio of TaC grains, higher volume fraction of amorphous carbon matrix and greater compressive stress in HiPIMS deposited films. These features responsible for better performance are supported by the greater degree of plasma reaction between Ta and C<sub>2</sub>H<sub>2</sub> due to the high energy density and high ionization rate of HiPIMS discharge. The application of substrate bias in HiPIMS further improves the mechanical properties and the wear resistance, but deteriorates the friction coefficient and oxidation resistance of the film. These performance adjustments result from two influences of enhanced ion bombardment. One is that it causes both the mobility of Ta ions and the reactivity with C to be further enhanced at the growing interface of the film. The volume fraction of amorphous carbon is thus lowered and the carbide volume fraction is increased, corresponding to the degradation of the friction coefficient. The other is that it results in the increased stoichiometric ratio of TaC grains, enhanced compressive stress, densification of the morphology, and coarsened grain. The first three promote optimization of mechanical

properties and wear resistance while the latter one inhibits the oxidation resistance of the film. It is demonstrated that HiPIMS provides a better strategy to tune the chemical bonding state and nanocomposite structure of TaC/a-C:H film through HiPIMS plasma in a way favorable for improving mechanical properties, tribological performance, and oxidation resistance. Moreover, it is very practical and can be transferred to other carbon-based protective films broader than that tested within the present article.

### Acknowledgments

The authors thank the China Scholarship Council (No. 201604490110) and Pays de Montbéliard Agglomeration for their financial support of this study.

### Additional information

Declarations of interest: none.

### References

- [1] H. Lasfargues, T. Glechner, C. M. Koller, V. Paneta, D. Primetzhofer, S. Kolozsvári, D. Holec, H. Riedl, P. H. Mayrhofer, Non-reactively sputtered ultra-high temperature Hf-C and Ta-C coatings, *Surf. Coat. Technol.* 309 (2017) 436-444. <https://doi.org/10.1016/j.surfcoat.2016.11.073>
- [2] S. H. Jhi, S. G. Louie, M. L. Cohen, J. Ihm, Vacancy hardening and softening in transition metal carbides and nitrides, *Phys. Rev. Lett.* 86 (2001) 3348. <https://doi.org/10.1103/PhysRevLett.86.3348>
- [3] H. Riedl, T. Glechner, T. Wojcik, N. Koutná, S. Kolozsvári, V. Paneta, D. Holec, D. Primetzhofer, P. H. Mayrhofer, Influence of carbon deficiency on phase formation and thermal stability of super-hard TaCy thin films, *Scr. Mater.* 149 (2018) 150-154. <https://doi.org/10.1016/j.scriptamat.2018.02.030>
- [4] E. K. Storms, *The Refractory Carbides*, Academic, New York, 1967.
- [5] S. L. Wang, K. Z. Li, H. J. Li, Y. L. Zhang, T. Feng, Structure evolution and ablation behavior of ZrC coating on C/C composites under single and cyclic oxyacetylene torch environment, *Ceram. Int.* 40 (2014) 16003-16014. <https://doi.org/10.1016/j.ceramint.2014.07.132>
- [6] Y. Wang, H. Li, Q. Fu, H. Wu, D. Yao, H. Li, SiC/HfC/SiC ablation resistant coating for carbon/carbon composites, *Surf. Coat. Technol.* 206 (2012) 3883-3887. <https://doi.org/10.1016/j.surfcoat.2012.03.039>

- [7] H. Pu, Y. Niu, C. Hu, G. Wang, H. Li, Y. Zeng, X. Zheng, Ablation of vacuum plasma sprayed TaC-based composite coatings, *Ceram. Int.* 41 (2015) 11387-11395. <https://doi.org/10.1016/j.ceramint.2015.05.100>
- [8] J. C. Sánchez-López, S. Dominguez-Meister, T. C. Rojas, M. Colasuonno, M. Bazzan, A. Patelli, Tribological properties of TiC/aC: H nanocomposite coatings prepared via HiPIMS, *Appl. Surf. Sci.* 440 (2018) 458-466. <https://doi.org/10.1016/j.apsusc.2018.01.135>
- [9] Z. Peng, H. Miao, L. Qi, S. Yang, C. Liu, Hard and wear-resistant titanium nitride coatings for cemented carbide cutting tools by pulsed high energy density plasma, *Acta Mater.* 51 (2003) 3085-3094. [https://doi.org/10.1016/S1359-6454\(03\)00119-8](https://doi.org/10.1016/S1359-6454(03)00119-8)
- [10] M. D. Abad, M. A. Muñoz-Márquez, S. El Mrabet, A. Justo, J. C. Sánchez-López, Tailored synthesis of nanostructured WC/aC coatings by dual magnetron sputtering, *Surf. Coat. Technol.* 204 (2010) 3490-3500. <https://doi.org/10.1016/j.surfcoat.2010.04.019>
- [11] S. El Mrabet, M. D. Abad, J. C. Sánchez-López, Identification of the wear mechanism on WC/C nanostructured coatings, *Surf. Coat. Technol.* 206 (2011) 1913-1920. <https://doi.org/10.1016/j.surfcoat.2011.07.059>
- [12] T. Zehnder, P. Schwaller, F. Munnik, S. Mikhailov, J. Patscheider, Nanostructural and mechanical properties of nanocomposite nc-TiC/a-C: H films deposited by reactive unbalanced magnetron sputtering. *J. Appl. Phys.* 95 (2004) 4327-4334. <https://doi.org/10.1063/1.1650898>
- [13] D. Martínez-Martínez, C. López-Cartes, A. Fernández, J. C. Sánchez-López, Influence of the microstructure on the mechanical and tribological behavior of TiC/aC nanocomposite coatings, *Thin Solid Films*, 517 (2009) 1662-1671. <https://doi.org/10.1016/j.tsf.2008.09.091>
- [14] K. Zhang, M. Wen, G. Cheng, X. Li, Q. N. Meng, J. S. Lian, W. T. Zheng, Reactive magnetron sputtering deposition and characterization of niobium carbide films, *Vacuum*, 99 (2014) 233-241. <https://doi.org/10.1016/j.vacuum.2013.06.012>
- [15] N. Nedfors, O. Tengstrand, E. Lewin, A. Furlan, P. Eklund, L. Hultman, U. Jansson, Structural, mechanical and electrical-contact properties of nanocrystalline-NbC/amorphous-C coatings deposited by magnetron sputtering, *Surf. Coat. Technol.* 206 (2011) 354-359. <https://doi.org/10.1016/j.surfcoat.2011.07.021>

- [16] X. M. He, L. Shu, H. B. Li, H. D. Li, S. T. Lee, Structural characteristics and hardness of zirconium carbide films prepared by tri-ion beam-assisted deposition, *J. Vac. Sci. Technol. A*. 16 (1998) 2337-2344. <https://doi.org/10.1116/1.581349>
- [17] K. Hackett, S. Verhoef, R. A. Cutler, D. K. Shetty, Phase constitution and mechanical properties of carbides in the Ta–C system, *J. Am. Ceram. Soc.* 92 (2009) 2404-2407. <https://doi.org/10.1111/j.1551-2916.2009.03201.x>
- [18] J. Hu, H. Li, J. Li, J. Kong, H. Zhu, D. Xiong, Structure, mechanical and tribological properties of TaC<sub>x</sub> composite films with different graphite powers, *J. Alloy. Compd.* (2020) 153769. <https://doi.org/10.1016/j.jallcom.2020.153769>
- [19] S. Du, K. Zhang, M. Wen, Y. Qin, R. Li, H. Jin, X. Bao, P. Ren, W. Zheng, Optimizing the tribological behavior of tantalum carbide coating for the bearing in total hip joint replacement, *Vacuum*, 150 (2018) 222-231. <https://doi.org/10.1016/j.vacuum.2018.01.050>
- [20] R. D. Evans, J. Y. Howe, J. Bentley, G. L. Doll, J. T. Glass, Influence of deposition parameters on the composition and structure of reactively sputtered nanocomposite TaC/aC: H thin films, *J. Mater. Res.* 20 (2005) 2583-2596. <https://doi.org/10.1557/jmr.2005.0324>
- [21] R. D. Evans, G. L. Doll, W. J. Meng, F. Mei, J. T. Glass, Effects of applied substrate bias during reactive sputter deposition of nanocomposite tantalum carbide/amorphous hydrocarbon thin films, *Thin solid films*, 515 (2007) 5403-5410. <https://doi.org/10.1016/j.tsf.2006.12.034>
- [22] T. Tokoroyama, T. Hattori, N. Umehara, H. Kousaka, K. Manabe, M. Kishi, Y. Fuwa, Ultra-low friction properties of carbon nitride tantalum coatings in the atmosphere. *Tribol. Int.* 103 (2016) 388-393. <https://doi.org/10.1016/j.triboint.2016.07.015>
- [23] A. Poladi, H. M. Semnani, E. Emadoddin, F. Mahboubi, H. R. Ghomi, Nanostructured TaC film deposited by reactive magnetron sputtering: Influence of gas concentration on structural, mechanical, wear and corrosion properties, *Ceram. Int.* 45 (2019) 8095-8107. <https://doi.org/10.1016/j.ceramint.2019.01.055>
- [24] X. Cai, Y. Xu, M. Liu, L. Zhong, F. Bai, Preparation of a gradient nanostructured surface TaC layer-reinforced Fe substrate by in situ reaction, *J. Alloy. Compd.* 712 (2017) 204-212. <https://doi.org/10.1016/j.jallcom.2017.04.081>

- [25] N. Zhao, Y. Xu, J. Wang, L. Zhong, V. E. Ovcharenko, X. Cai, Microstructure and kinetics study on tantalum carbide coating produced on gray cast iron in situ, *Surf. Coat. Technol.* 286 (2016) 347-353.  
<https://doi.org/10.1016/j.surfcoat.2015.12.057>
- [26] Z. Zhao, P. Hui, F. Liu, X. Wang, B. Li, Y. Xu, L. Zhong, M. Zhao, Fabrication of TaC coating on tantalum by interstitial carburization, *J. Alloy. Compd.* 790 (2019) 189-196.  
<https://doi.org/10.1016/j.jallcom.2019.03.164>
- [27] D. Cotton, P. Jacquet, S. Faure, V. Vignal, Epitaxial growth of tantalum carbides by low carbon flow carburizing, *Mater. Chem. Phys.* 192 (2017) 170-180. <https://doi.org/10.1016/j.matchemphys.2016.12.063>
- [28] R. Teghil, A. De Bonis, A. Galasso, P. Villani, A. Santagata, Femtosecond pulsed laser ablation deposition of tantalum carbide, *Appl. Surf. Sci.* 254 (2007) 1220-1223.  
<https://doi.org/10.1016/j.apsusc.2007.07.178>
- [29] R. Teghil, L. D'Alessio, M. Zaccagnino, D. Ferro, V. Marotta, G. De Maria, TiC and TaC deposition by pulsed laser ablation: a comparative approach, *Appl. Surf. Sci.* 173 (2001) 233-241.  
[https://doi.org/10.1016/S0169-4332\(00\)00900-4](https://doi.org/10.1016/S0169-4332(00)00900-4)
- [30] D. Ferro, J. V. Rau, V. R. Albertini, A. Generosi, R. Teghil, S. M. Barinov, Pulsed laser deposited hard TiC, ZrC, HfC and TaC films on titanium: hardness and an energy-dispersive X-ray diffraction study, *Surf. Coat. Technol.* 202 (2008) 1455-1461. <https://doi.org/10.1016/j.surfcoat.2007.06.060>
- [31] Y. Long, A. Javed, J. Chen, Z. K. Chen, X. Xiong, The effect of deposition temperature on the microstructure and mechanical properties of TaC coatings, *Mater. Lett.* 121 (2014) 202-205.  
<https://doi.org/10.1016/j.matlet.2014.01.145>
- [32] M. Ali, M. Ürgen, Tantalum carbide-graphite composite film synthesized by hot-filament chemical vapor deposition, *Pure Appl. Chem.* 84 (2012) 2499-2506. <https://doi.org/10.1351/PAC-CON-11-12-01>
- [33] L. Massot, P. Chamelot, P. Taxil, Preparation of tantalum carbide films by reaction of electrolytic carbon coating with the tantalum substrate, *J. Alloy. Compd.* 424 (2006) 199-203.  
<https://doi.org/10.1016/j.jallcom.2005.09.095>

- [34] W. Shuo, Z. Kan, A. Tao, H. Chaoquan, M. Qingnan, M. Yuanzhi, W. Mao, Z. Weitao, Structure, mechanical and tribological properties of HfCx films deposited by reactive magnetron sputtering, *Appl. Surf. Sci.* 327 (2015) 68-76. <https://doi.org/10.1016/j.apsusc.2014.11.130>
- [35] A. A. Voevodin, M. A. Capano, A. J. Safriet, M. S. Donley, J. S. Zabinski, Combined magnetron sputtering and pulsed laser deposition of carbides and diamond - like carbon films, *Appl. Phys. Lett.* 69 (1996) 188-190. <https://doi.org/10.1063/1.117367>
- [36] P. Souček, J. Daniel, J. Hnilica, K. Bernátová, L. Zábranský, V. Buršíková, M. Stupavská, P. Vašina, Superhard nanocomposite nc-TiC/aC: H coatings: The effect of HiPIMS on coating microstructure and mechanical properties, *Surf. Coat. Technol.* 311 (2017) 257-267. <https://doi.org/10.1016/j.surfcoat.2017.01.021>
- [37] K. M. Jiang, D. Q. Zhao, X. Jiang, Q. Huang, L. J. Miao, H. M. Lu, Y. Li, Electronic-structure, corrosion and mechanical properties of nc-CrC/aC: H films deposited by multi-arc ion plating, *J. Alloy. Compd.* 750 (2018) 560-569. <https://doi.org/10.1016/j.jallcom.2018.04.017>
- [38] M. Samuelsson, K. Sarakinos, H. Högberg, E. Lewin, U. Jansson, B. Wälivaara, H. Ljungcrantz, U. Helmersson, Growth of Ti-C nanocomposite films by reactive high power impulse magnetron sputtering under industrial conditions, *Surf. Coat. Technol.* 206 (2012) 2396-2402. <https://doi.org/10.1016/j.surfcoat.2011.10.039>
- [39] J. Alami, P. Å. Persson, D. Music, J. T. Gudmundsson, J. Bohlmark, U. Helmersson, Ion-assisted physical vapor deposition for enhanced film properties on nonflat surfaces, *J. Vac. Sci. Technol. A* 23 (2005) 278-280. <https://doi.org/10.1116/1.1861049>
- [40] J. C. Oliveira, F. Ferreira, A. Anders, A. Cavaleiro, Reduced atomic shadowing in HiPIMS: Role of the thermalized metal ions, *Appl. Surf. Sci.* 433 (2018) 934-944. <https://doi.org/10.1016/j.apsusc.2017.10.133>
- [41] V. J. Benavides, C. D. Salazar, M. E. Espitia, D. M. Devia, A. Devia, Study of TiC/aC thin films growth by cathodic arc discharge varying the substrate temperature. *Phys. Scr. T131* (2008) 014021. <https://doi.org/10.1088/0031-8949/2008/T131/014021>

- [42] E. Lewin, P. Å. Persson, M. Lattemann, M. Stüber, M. Gorgoi, A. Sandell, ... & S. Ulrich, On the origin of a third spectral component of C1s XPS-spectra for nc-TiC/aC nanocomposite thin films, *Surf. Coat. Technol.* 202 (2008) 3563-3570. <https://doi.org/10.1016/j.surfcoat.2007.12.038>
- [43] D. Galvan, Y. T. Pei, J. T. M. De Hosson, Influence of deposition parameters on the structure and mechanical properties of nanocomposite coatings, *Surf. Coat. Technol.* 201 (2006) 590-598. <https://doi.org/10.1016/j.surfcoat.2005.12.007>
- [44] Y. Hu, L. Li, X. Cai, Q. Chen, P. K. Chu, Mechanical and tribological properties of TiC/amorphous hydrogenated carbon composite coatings fabricated by DC magnetron sputtering with and without sample bias, *Diam. Relat. Mat.* 16 (2007) 181-186. <https://doi.org/10.1016/j.diamond.2006.05.010>
- [45] J. Patscheider, Nanocomposite hard coatings for wear protection, *MRS bull.* 28 (2003) 180-183. <https://doi.org/10.1557/mrs2003.59>
- [46] Q. J. Hong, A. van de Walle, Prediction of the material with highest known melting point from ab initio molecular dynamics calculations, *Phys. Rev. B*, 92 (2015) 020104. <https://doi.org/10.1103/PhysRevB.92.020104>
- [47] J. Musil, Hard nanocomposite coatings: Thermal stability, oxidation resistance and toughness, *Surf. Coat. Technol.* 207 (2012) 50-65. <https://doi.org/10.1016/j.surfcoat.2012.05.073>
- [48] J. Blažek, J. Musil, P. Stupka, R. Čerstvý, J. Houška, Properties of nanocrystalline Al–Cu–O films reactively sputtered by DC pulse dual magnetron, *Appl. Surf. Sci.* 258 (2011) 1762-1767. <https://doi.org/10.1016/j.apsusc.2011.10.039>
- [49] A. A. Voevodin, J. S. Zabinski, Load-adaptive crystalline–amorphous nanocomposites, *J. Mater. Sci.* 33 (1998) 319-327. <https://doi.org/10.1023/A:1004307426887>
- [50] A. A. Voevodin, J. S. Zabinski, Supertough wear-resistant coatings with ‘chameleon’ surface adaptation, *Thin Solid Films*, 370 (2000) 223-231. [https://doi.org/10.1016/S0040-6090\(00\)00917-2](https://doi.org/10.1016/S0040-6090(00)00917-2)
- [51] L. E. Toth, *Transition Metal Carbides and Nitrides*, Academic Press, New York, 1971.
- [52] H. Holleck, *Material selection for hard coatings*, *J. Vac. Sci. Technol. A*. 4 (1986) 2661-2669. <https://doi.org/10.1116/1.573700>

- [53] A. Banerji, S. Bhowmick, A. T. Alpas, High temperature tribological behavior of W containing diamond-like carbon (DLC) coating against titanium alloys, *Surf. Coat. Technol.* 241 (2014) 93-104.  
<https://doi.org/10.1016/j.surfcoat.2013.10.075>
- [54] D. Yanchun, Y. Dianran, H. Jining, Z. Jianxin, X. Lisong, L. Xiangzhi, Studies on nanocrystalline TiN coatings prepared by reactive plasma spraying, *J. Nanomater.* 45 (2008).  
<https://doi.org/10.1155/2008/690951>
- [55] K. Zhang, M. Wen, Q. N. Meng, C. Q. Hu, X. Li, C. Liu, W. T. Zheng, Effects of substrate bias voltage on the microstructure, mechanical properties and tribological behavior of reactive sputtered niobium carbide films, *Surf. Coat. Technol.* 212 (2012) 185-191. <https://doi.org/10.1016/j.surfcoat.2012.09.046>
- [56] Y. T. Pei, D. Galvan, J. T. M. De Hosson, Nanostructure and properties of TiC/aC: H composite coatings, *Acta Mater.* 53 (2005) 4505-4521. <https://doi.org/10.1016/j.actamat.2005.05.045>
- [57] J. Musil, F. Kunc, H. Zeman, H. Polakova, Relationships between hardness, Young's modulus and elastic recovery in hard nanocomposite coatings, *Surf. Coat. Technol.* 154 (2002) 304-313.  
[https://doi.org/10.1016/S0257-8972\(01\)01714-5](https://doi.org/10.1016/S0257-8972(01)01714-5)
- [58] J. Musil, M. Jirout, Toughness of hard nanostructured ceramic thin films, *Surf. Coat. Technol.* 201 (2007) 5148-5152. <https://doi.org/10.1016/j.surfcoat.2006.07.020>
- [59] N. P. Suh, An overview of the delamination theory of wear, *Wear*, 44 (1977) 1-16.  
[https://doi.org/10.1016/0043-1648\(77\)90081-3](https://doi.org/10.1016/0043-1648(77)90081-3)
- [60] H. J. Li, Q. G. Fu, X. H. Shi, K. Z. Li, Z. B. Hu, SiC whisker-toughened SiC oxidation protective coating for carbon/carbon composites, *Carbon*, 3 (2006) 602-605.  
<https://doi.org/10.1016/j.carbon.2005.09.026>

## Figures

Figure 1. High resolution XPS spectra C 1s of TaC/a-C:H films deposited in different conditions: (a) DC; (b) HiPIMS with floating substrate; (c) HiPIMS with substrate bias.

Figure 2. SEM micrographs of cross-sections and top surfaces (upper right corner) of TaC/a-C:H films deposited in DC (upper row, a-c) and in HiPIMS (lower row, d-f) with various C<sub>2</sub>H<sub>2</sub> flow rates: (a, d) 10 sccm, (b, e) 14 sccm and (c, f) 16 sccm.

Figure 3. SEM micrographs of top surfaces (a-c) and of cross-sections (d-f) of HiPIMS deposited TaC/a-C:H films at 16 sccm C<sub>2</sub>H<sub>2</sub> with different substrate bias: (a) floating, (b) -50 V, (c) -100 V.

Figure 4. X-ray diffractograms of TaC/a-C:H films deposited in DC (left) and HiPIMS (right).

Figure 5. The grain size of TaC/a-C:H films deposited in different conditions with various C<sub>2</sub>H<sub>2</sub> flow rates.

Figure 6. The HRTEM images and corresponding SAED patterns of TaC/a-C:H films deposited in DC with (a) 12 sccm (b) 16 sccm and (c) 18 sccm and in HiPIMS with (d) 16 sccm C<sub>2</sub>H<sub>2</sub> flow rates.

Figure 7. Hardness H and Young's modulus E of TaC/a-C:H films with various C<sub>2</sub>H<sub>2</sub> flow rate.

Figure 8. Ratio H/E and compressive stress of TaC/a-C:H films as a function of C<sub>2</sub>H<sub>2</sub> flow rate.

Figure 9. Friction coefficients of TaC/a-C:H films deposited in different conditions as a function of sliding cycle: (a) DC, (b) HiPIMS with floating substrate, (c) HiPIMS with different substrate bias (at 16 sccm C<sub>2</sub>H<sub>2</sub>).

Figure 10. Friction coefficient (lines) and wear rate (columns) of TaC/a-C:H films as a function of C<sub>2</sub>H<sub>2</sub> flow rate.

Figure 11. Wear tracks of TaC/a-C:H films deposited in DC (group I) and HiPIMS (group II). In both groups, (a), (b) and (c) represent the films prepared at 12 sccm, 16 sccm and 18 sccm C<sub>2</sub>H<sub>2</sub>, where (d), (e), (f) are magnified views of the white squared regions in (a), (b), (c). The EDS maps of the subgraph (f) are displayed on the right side of group II.

Figure 12. SEM images and cross profiles of wear tracks for HiPIMS TaC/a-C:H films deposited at 12 sccm C<sub>2</sub>H<sub>2</sub> flow rate with different substrate bias: (a-c) floating, (b-f) -50 V, (g-i) -100 V.

Figure 13. X-ray diffractograms of the TaC/a-C:H films deposited in different conditions as a function of annealing temperature: (a) DC, (b) HiPIMS with floating substrate, (c) HiPIMS with -100 V bias.

Figure 14. SEM/EDS images of cross-sections of TaC/a-C:H films after annealing temperature at 600 °C: (a) DC, (b) HiPIMS with floating substrate, and (c) HiPIMS with -100 V bias.

#### **Tables**

Table 1. The relative amount of chemical bonds of Ta-C,  $sp^2$ -C and  $sp^3$ -C, stoichiometric ratio  $x$  of TaC grains, and amorphous carbon content of the TaC/a-C:H films with different  $C_2H_2$  flow rates.